

Luminescent Silicon Nanoparticles:  
An improved inverse micelle synthesis and  
oxide-dependent photoluminescence studies

November 16, 2015



Frederik Huld  
100044585



## Abstract

The luminescence of silicon nanoparticles has been an active area of study for a number of years. These nanoparticles luminesce when excited by ultraviolet (UV) light in the ~340 nm region, displaying either a blueish or a reddish colour. The control and origin of these colours has been debated, with researchers such as Veinot, Kauzlarich and Tilley claiming that the luminescence can be controlled with the use of nitrogen. In this thesis, a new synthetic procedure is presented that improves upon the established inverse-micelle technique by replacing the methanol or ethanol quenching agent with copper chloride. It is found that this new technique lowers the level of surface oxide present in the form of alcohols on the surface of the nanoparticles, giving blue luminescent particles with improved surfaces for further chemistry.

Photoluminescence studies are also performed on samples of silicon nanoparticles synthesised by electrochemical etching, using a variety of oxygen-containing compounds to probe the behaviour of the photoluminescence spectrum. It is found that there are typically five Gaussian peaks present in a typical spectrum; occurring at 405 nm, 430 nm, 460 nm, 485-90 nm, 500 nm, and 640 nm, subsequently labelled  $\alpha$ ,  $\beta$ ,  $\gamma$ ,  $\epsilon$ , and  $\zeta$ . It is also found that molecular oxygen increases the  $\beta$  peak and suppresses the  $\zeta$  peak, and that water has the opposite effect on these two peaks. It is shown that the peaks  $\alpha$ ,  $\beta$ , and  $\zeta$  are all due to a single site on the surface of the silicon nanoparticle, corresponding to the cases when the site is oxide-free, occupied by molecular oxygen, and water, respectively. It is also hypothesised that the luminescence can be controlled *via* the use of compounds of different sizes and polarities, with electron-withdrawing molecules increasing the blue luminescence, and electron-donating molecules increasing the red.  $\gamma$  and  $\epsilon$  are used as normalising peaks to compare between samples, and are not affected by oxygen.



## Acknowledgements

The following people were integral to the success of this project. While the words used to express my gratitude may be few, they are nonetheless sincere and heartfelt.

- My primary supervisor Dr Yimin Chao, for his trust, patience, and calming presence. I am a better scientist today as a result of his efforts.
- Kate Collingridge, for her caring patience and support throughout this thesis.
- Christine Collingridge, for many helpful discussions and much-needed motivation and support.
- Dr Shane Ashby, whose passion for the subject of nanoscience and many useful and stimulating discussions helped guide this work.
- Current and former members of the Chao group: Mehrnaz Behray, Jayshree Ahire, Ting Li, Tiezheng Bhan, and Qi Wang.
- Members of the Wildgoose group, especially Drs Elliot Lawrence and Robin Blagg.
- Jason Thomas and Professor Christopher Pickett



# Contents

<b>1</b>	<b>Introduction</b>	<b>1</b>
1.1	Silicon in nanoscience . . . . .	1
1.2	Traps, surface states and phonons . . . . .	4
1.3	Scattering . . . . .	4
1.4	Colour . . . . .	5
1.5	Methods for characterising nanoparticles . . . . .	7
1.6	Objectives . . . . .	8
<b>2</b>	<b>Synthesis of SiNPs</b>	<b>9</b>
2.1	General synthesis of RSiNPs by chemical reduction of micelles . . . . .	9
2.1.1	Synthesis of CuCl <sub>2</sub> -quenched, dodecyl-capped SiNPs: . . . . .	11
2.1.2	Machine specifications for characterisation . . . . .	12
2.2	General synthesis of HSiNPs by electrochemical etching . . . . .	13
2.2.1	Synthesis of hydrogen-capped SiNPs: . . . . .	13
<b>3</b>	<b>CuCl<sub>2</sub>-quenched SiNPs</b>	<b>15</b>
<b>4</b>	<b>Photoluminescence of SiNPs</b>	<b>23</b>
4.1	Photoluminescence characterisation of HSiNPs . . . . .	23
4.2	Time-dependent photoluminescence of HSiNPs . . . . .	32
4.3	Discussion . . . . .	33
<b>5</b>	<b>Conclusions and further work</b>	<b>35</b>

# *CONTENTS*

## List of Figures

1	Graphical representations of a trap (a), surface states (b) and an optical phonon (c), as well as fluorescent decay (d). The subscripts <i>i</i> , and <i>o</i> stand for in and out, respectively. . . . .	5
2	Refraction (a) and scattering (b) of light by particles of similar size to the wavelength of incident light. The subscripts <i>i</i> , <i>s</i> , and <i>o</i> stand for in, scattered, and out, respectively. . . . .	5
3	The effect on the band structure of a semiconductor as the size of the particle reaches the de Broglie wavelength. . . . .	6
4	Diagrammatic representation of the synthesis of SiNPs by chemical reduction of micelles. . . . .	10
5	A hypothetical depiction of the changes in surface chemistry as a result of quenching with alcohol (a), or CuCl <sub>2</sub> (b). . . . .	11
6	Electrochemical etching cell used for production of hydrogen-capped SiNPs .	14
7	FTIR spectrum for CuCl <sub>2</sub> -quenched, dodecyl-capped SiNPs. . . . .	17
8	NMR spectrum for CuCl <sub>2</sub> -quenched, dodecyl-capped SiNPs. . . . .	18
9	XPS spectrum for CuCl <sub>2</sub> -quenched, dodecyl-capped SiNPs. The inset is the high-resolution Si2p peak. . . . .	19
10	Image of CuCl <sub>2</sub> -quenched, dodecyl-capped SiNPs under UV irradiation at 365 nm. . . . .	19
11	PL spectrum of CuCl <sub>2</sub> -quenched, dodecyl-capped SiNPs: the black line is the excitation spectrum measured as the response of the emission at 420 nm, while the red line is the emission spectrum with an excitation wavelength of 345 nm. . . . .	20
12	UV–Vis spectrum of CuCl <sub>2</sub> -quenched, dodecyl-capped SiNPs. . . . .	20
13	Integrated PL intensity against absorbance for diluted dodecyl-capped SiNPs in hexane and quinine sulphate in 1 M H <sub>2</sub> SO <sub>4</sub> solution for QY measurement, collected under the excitation at 340 nm and ambient conditions. . . . .	21
14	PL decay spectra monitored over 21 days with excitation wavelength of 340 nm.	21
15	Aberration-corrected STEM images of the SiNPs made using the inversed micellar method quenched through introduction of CuCl <sub>2</sub> . Inset is a high-resolution TEM image with visible crystal nature of a SiNP. . . . .	22
16	FTIR comparison of MeOH-quenched SiNPs (top), EtOH-quenched (middle), and CuCl <sub>2</sub> -quenched, dodecyl-capped SiNPs (bottom) . . . . .	22

LIST OF FIGURES

17 Example of the Photoluminescence of SiNPs at an excitation wavelength of 340 nm, with a superimposed multiple Gaussian fit. The blue line is the raw data, the red lines are the component Gaussians that together make up the fitting function, and the dotted red line is the resulting fit.  $R^2 = 0.998$  . . . . . 25

18 PL spectra of HSiNPs dispersed in toluene, comparing levels of oxygen and water in toluene (a), and levels of oxygen and water with added ethanol (b). . . . . 28

19 PL comparison of HSiNPs dispersed in toluene, with the maxima of the fitted peaks superimposed over the top. The three curves are neat toluene (blue line, blue dots), distilled toluene (dark cyan line, dark cyan squares), and toluene that had been both distilled and then degassed (cyan line, cyan diamonds). The dotted lines are for ease of visualisation only. . . . . 29

20 . . . . . 30

20 Plots of the PL spectra for HSiNPs made by electrochemical etching. The four graphs describe the behaviour of the addition of: alcohols to HSiNPs dispersed in neat toluene (a); phenols to HSiNPs dispersed in neat toluene (b); alcohols to HSiNPs dispersed in distilled toluene (c); and alcohols to HSiNPs in distilled and degassed toluene (d). . . . . 31

21 Progression of the intensity of luminescence of peaks  $\alpha$ ,  $\beta$ ,  $\epsilon$ , and  $\zeta$  (red, blue, green, and black lines respectively) with time for a sample of HSiNPs dispersed in neat toluene with added phenol, with a 1-hour moving average. . . . . 32

# 1 Introduction

Nanomaterials, defined as materials with a physical dimension between 1-100nm as defined by the National Nanotechnology Initiative,<sup>1</sup> have long been used by humankind. The Egyptians and Romans used lead sulfide nanoparticles for dyeing their hair more than 4000 years ago,<sup>2</sup> and the vivid red in stained-glass windows has been shown to originate from gold nanoparticles less than 100 nm in diameter.<sup>3</sup> In more modern times, titania nanoparticles have been added to plastics to prevent degradation from UV light.<sup>4</sup>

Nanotechnology, the study and manipulation of nanomaterials, first became popular in the late 1980's and early 1990's with several publications on the subject<sup>5-7</sup> including the launch of Nanotechnology in 1990.<sup>8</sup>

Since then, the field of nanotechnology has grown to encompass all fields of science, from biology and environment,<sup>9-11</sup> to medicine,<sup>12-14</sup> to energy generation and storage.<sup>15-19</sup>

In this relatively short period of time, the fruits of the labour of researchers across the globe have shown themselves in day-to-day life, with the Consumer Products Inventory listing more than 1600 "manufacturer-identified nanotechnology-based consumer products".<sup>20</sup> These products range from corrosion-protected coatings to metabolic aids and include almost every product category.

The interest in nanomaterials stems in part from the many properties displayed by materials once they reach the nano-scale region. These properties are not displayed in bulk, such as optical properties arising from their small size, and functionalities not present as molecules.<sup>21-23</sup> Nanoparticles, for example, have a very high surface to core ratio, along with very strained bonds, leading to unusual chemical and optical properties.<sup>24,25</sup>

One promising aspect of nanotechnology is the application of nanoparticles in medicine, for example as biomarkers,<sup>13,14</sup> or as drug carriers for fighting cancer.<sup>12,14</sup> However, many of the more synthetically amenable and well-researched nanoparticles require either relatively expensive starting materials (such as gold) or are very toxic, such as CdSe.<sup>26</sup> Because of this, it has become necessary to find and understand types of nanoparticles that avoid these problems, while still having desirable optical and physical properties.

## 1.1 Silicon in nanoscience

Recently, interest has arisen in the properties of Silicon in the nano-region. The hydrolysed surface of silicon can, for example, be functionalised by the addition of lithiated molecules.<sup>12,15,16</sup> This is useful for medical applications as it allows for the attachment of drugs to the surface of the nanoparticles.<sup>12,15,16</sup> Silicon is also non-toxic compared to other nanoparticles such as CdSe.<sup>26</sup> Optically, Silicon nanoparticles (SiNPs) are fluorescent, glowing either blue/green or

red/orange when excited by near-UV light.<sup>24,27–29</sup> The origin of this luminescence is poorly understood, however, with disagreement on the origin of each process.<sup>24,27–31</sup> These disagreements arise from the difficult characterisation of these nanoparticles. SiNPs are not neatly spherical, nor are they particularly crystalline, containing a high proportion of highly strained bond angles.<sup>32</sup> Unfunctionalised SiNPs are also very reactive, oxidising readily to form silica on the surface.<sup>15,16</sup> Thus, there are many avenues to explore when determining the luminescence of SiNPs.

Broadly speaking, SiNPs can be divided into two parts: the core, comprised of crystalline silicon, with no exposure to the outside chemical environment; and the surface, comprised of surface states and defects, such as strained bonds and bond angles, impurities such as oxides, and dangling bonds. As is implied by the name, the surface is in contact with the surrounding environment, and its properties are therefore highly dependent on it. Unfortunately, due to the highly strained nature of the particle, the boundary between the surface and the core is difficult to define both conceptually and physically. For instance, the computational studies performed by Barnard show that there is not really any such thing as a crystalline (i.e. regularly diamond cubics) portion of the SiNP for nanoparticles of ~5 nm, as the bond angle distribution varies from 80-130°, and the average crystal size is <4Å.<sup>32</sup> While this does not preclude the existence of a core portion of the nanoparticle with bulk-like (i.e. a high concentration of 109.5° bond angles) physical appearance, it does suggest that this 'core' may be so small as to be potentially negligible. Any experiment that proves the existence of the 'core' would therefore be one where the surface properties are affected but the 'core' is not. This would be possible through the addition of certain types of chemicals to the nanoparticle and monitoring the changes in – say optical – properties. However, care must be taken that unreactive surface properties are not mischaracterised.

In the past, research groups such as the one headed by Jonathan Veinot at the University of Alberta, Canada, or the one headed by Susan Kauzlarich at the University of California, have suggested a number of reasons why SiNPs display their distinctive colours. In 2013 Veinot and Kauzlarich, together with Richard Tilley (of Victoria University in Wellington, NZ), wrote a paper claiming that nitrogen and oxygen, naturally present in SiNPs due to the manufacturing process, causes the blue luminescence.<sup>30</sup> They showed that red luminescent SiNPs could be “switched” from red to blue by the simple addition of a solution of ammonium bromide (NH<sub>4</sub>Br) or tetraoctylammonium bromide (TOAB). They explain that the nitrogen atoms are bonded to the silicon surface to form either silicon amide or silicon dioctylamide, respectively. However, the increase in blue luminescence due to nitrogen does not explain why the red luminescence is destroyed.

Knowledge of the behaviour of SiNPs in different chemical environments would not just further our understanding of the chemistry of these particles, but it would be a valuable tool

to tune nanoparticle colour and brightness for medical imaging purposes.

Silicon, an abundant, cheap and non-toxic element, is primarily known for its applications in the semiconductor industry. However, there is an ever growing research interest looking at its nanoscale properties. Silicon is also an attractive material due to its low toxicity and chemical stability.<sup>33,34</sup> In terms of optical activity, silicon nanoparticles (SiNPs) demonstrate indirect band gap photoluminescence (PL), whereby quantum confinement effects, as well as surface structure and termination, have an effect on the PL mechanism.<sup>35–37</sup> Compared to direct band gap semiconductors, SiNPs generally exhibit a PL with long lifetime and low efficiencies.<sup>15,24,38,39</sup> Overall, SiNPs demonstrate physical and chemical properties largely different to those of bulk silicon, with behaviour dependent on their small size. It is these unique properties that lend silicon to new and exciting applications and research possibilities.<sup>40–44</sup> Researchers are currently involved in developing a diverse array of possible SiNP applications, including in fields such as photovoltaics;<sup>40</sup> thermoelectrics,<sup>45</sup> - due to semiconductor physical and chemical properties - and also exploiting biologically viable properties - such as low toxicity - for potential use in biological applications, including things such as drug delivery and bioimaging.<sup>12–14</sup> SiNPs, despite having this abundance of positive applications and features, do, however, find themselves lacking with respect to their synthesis. Although a great many methods for the synthesis of different types of SiNPs have been proposed and proven in practice, they often involve the use of expensive or toxic reagents or catalysts, are slow, or result in very polydisperse systems, where monodispersity and consistency is often paramount.<sup>34</sup> Established methods include approaches such as Silane decomposition<sup>27,33</sup> and electrochemical etching and sonication.<sup>24</sup> Solution synthesis methods and the formation of inverse micelles form the background for the method proposed here.<sup>15,46</sup> In an attempt to address the difficult consistency in synthesis, a recent method demonstrates a facile one pot, inverse micelle method for the synthesis of SiNPs that is cheap, fast, high yielding and produces spherical crystalline SiNPs.<sup>15</sup> These particles are alkyl passivated, with a core diameter of ~7 nm, demonstrating a strong, stable blue PL (420 nm) when excited with UV light (340 nm).<sup>15</sup> However, this synthesis method also demonstrated limitations. The method found problems with optimisation of the surface functionality of the particles. The particles produced demonstrate residual Si–H termination rather than the desired Si-alkyl termination, particularly with the use of alkyl-chained surfactants with more than 8–10 carbon–carbon links, leaving a number of “uncapped” sites - sites which remain susceptible to oxidative attack. Although it would be naive to think that “complete” alkyl capping could occur, the ratio of desirable to undesirable surface coverage can certainly be improved. In addition, this residual Si–H termination lead to a secondary problem, whereby alcohols used to quench excess  $\text{LiAlH}_4$  at the end of the reaction also react with the particle surfaces at these Si–H sites. The result is alkoxy capping, i.e. undesirable and seemingly unavoidable surface oxidation

formed during the synthesis, causing an undesirable multi-functionality in the product.<sup>47</sup> Using an inorganic salt such as  $\text{CuCl}_2$ , as demonstrated by Dung and Jeong (2012)<sup>48</sup>, could help to solve this problem. The solid Cu left behind as a result of the quenching reaction of  $\text{LiAlH}_4$  and  $\text{CuCl}_2$  can be removed by centrifugation or filtration.

## 1.2 Traps, surface states and phonons

The colours present when a nanoparticle is illuminated may be due to a variety of factors. Excited electrons may decay into energy levels from which they cannot easily escape. These energy levels are known as 'traps'.<sup>31</sup> An energy diagram demonstrating this is shown in Figure 1a.

'Surface state' applies to any impurity or defect in the surface, such as dangling or strained bonds, oxides, or unusually positioned atoms.<sup>24</sup> A variety of defect, including oxides and cracks in the surface, are shown in Figure 1b. Excitation in these defects may give rise to colours not observed in the bulk, as they are highly concentrated relative to the bulk. Colours arising from these defects could be modified by the chemical environment, or other processes that interfere with the surface of the nanoparticle.

Phonons are quasiparticles, vibrational excitations made up of several atoms. If the frequencies of these phonons are sufficiently high, scattering of light can occur. This is especially true for surface phonons, which are hindered by the surface defects. In nanoparticles the effect of surface phonons is very important to the optical and electronic properties due to the large ratio of surface to core.<sup>49</sup> Figure 1c shows a representation of an optical phonon, where different atoms are vibrating out of phase.

The final panel in figure 1 - d - displays fluorescent decay. This is a simplified demonstration of figures 1a and b, as the results of both of these leads to the emission of light at a lower energy than the incident light. Note that fluorescent decay is not necessarily due to surface states, but may be due to the structure of the nanoparticle.

## 1.3 Scattering

When light hits a particle, it is scattered. This scattering is described by Mie theory, and the degree of scattering is dependent on the wavelength of the incident light, the refractive indices of the particle and the matrix in which it is suspended, as well as the size of the particle. If the wavelength and polarization of the incident light is known, as well as the necessary refractive indices, it is possible (if difficult) to determine the size of the particle. In most light-based size determinations, the particles in question are assumed to be spherical. Unfortunately, once particles reach the nano-region, it is often difficult to justify this assumption. Additionally, nanoparticles that are decorated or that have significant reordering of the

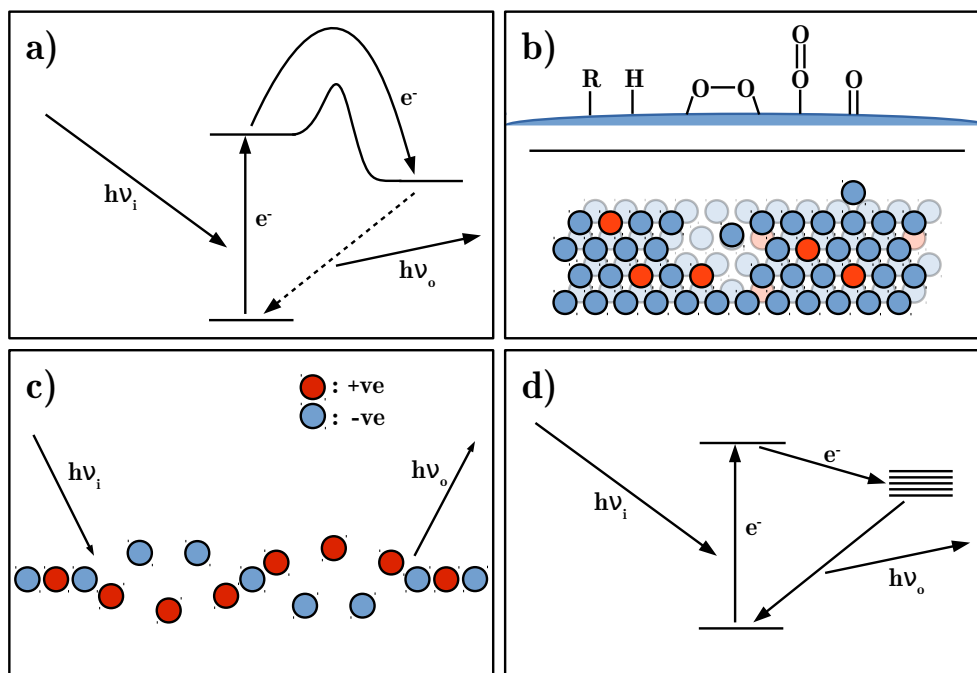


Figure 1: Graphical representations of a trap (a), surface states (b) and an optical phonon (c), as well as fluorescent decay (d). The subscripts  $i$ , and  $o$  stand for in and out, respectively.

surface do not necessarily have the same refractive index as that of the bulk material.

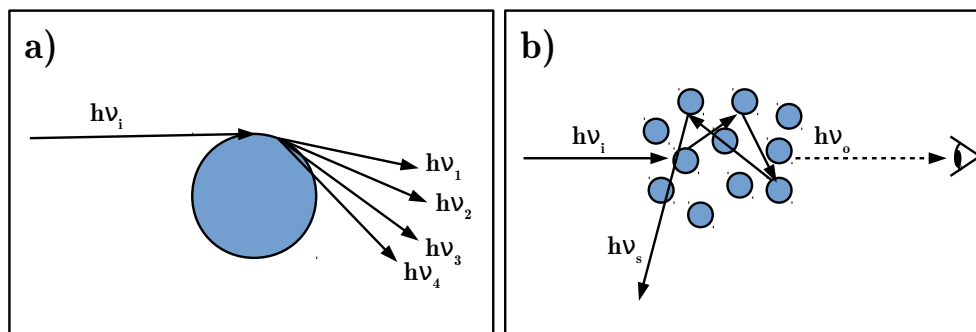


Figure 2: Refraction (a) and scattering (b) of light by particles of similar size to the wavelength of incident light. The subscripts  $i$ ,  $s$ , and  $o$  stand for in, scattered, and out, respectively.

## 1.4 Colour

Nanoparticles exhibit a large range of colours not displayed by bulk amounts of the same property. For example, CdSe nanoparticles can display a whole spectrum of colours depending on their size.<sup>21</sup>

Nanoparticles may exhibit different optical properties either due to quantum confinement, or due to the increased surface tension. In the case of the former, particles with a size smaller

than the de Broglie wavelength exhibit blueshift of their emission spectrum due to an increase in the band gap energy. This is displayed in Figure 3, which shows how the energy spectrum becomes discrete rather than continuous, which gives some of the very different optical properties seen in nanoparticles compared to the bulk.

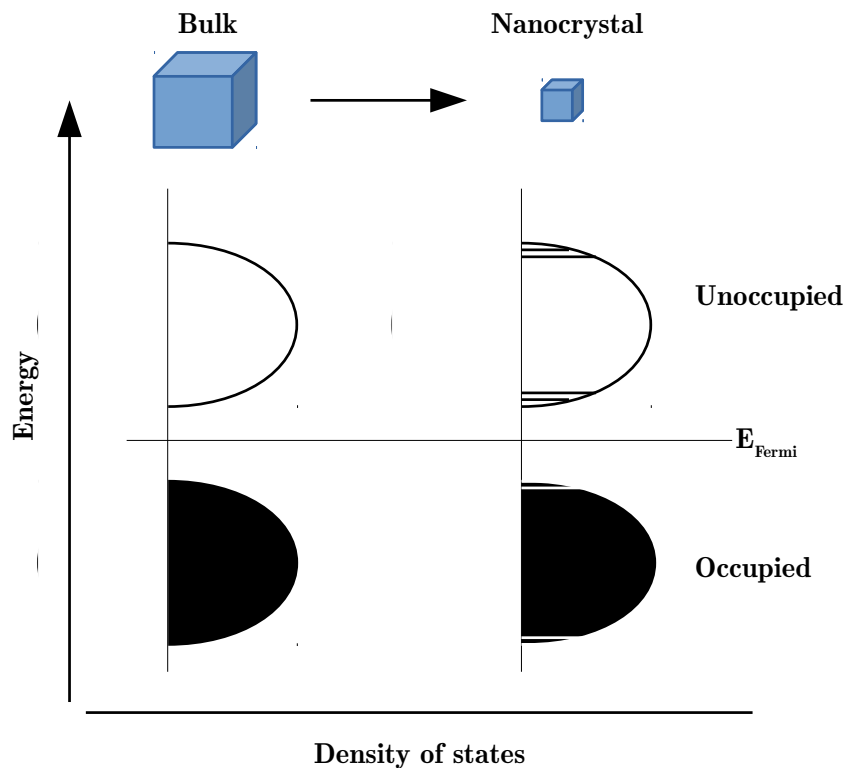


Figure 3: The effect on the band structure of a semiconductor as the size of the particle reaches the de Broglie wavelength.

In the second case, the pressure on the surface of a spherical particle is given by the Young-Laplace equation:

$$\Delta p = \frac{2\gamma}{R} \quad (1)$$

where  $\Delta p$  is the pressure difference over the (fluid) interface,  $\gamma$  is the surface tension on the surface and  $R$  is the radius of the particle. This means that nanoparticles have very large pressures acting across their surfaces (in the  $10^6 - 10^9 \text{ Nm}^{-1}$  range). As a result, the surface atoms may be quite distorted compared to the bulk, leading to the large bond angle discrepancy modelled by Barnard.<sup>32</sup>

Of ever growing interest in the fields of physical chemistry and materials science, silicon nanoparticles show a great deal of potential. Methods for their synthesis are, however, often hazardous, expensive or otherwise impractical. In the literature, there is a safe, fast and cheap inverse micelle-based method for the production of alkyl-functionalized blue luminescent silicon nanoparticles, which nonetheless found limitations, due to undesirable Si-alkoxy

and remaining Si–H functionalization. In the following work, these problems are addressed, whereby an optimisation of the reaction mechanism encourages more ‘desirable’ capping, and the introduction of alcohol is replaced by the use of anhydrous copper (II) chloride. The resulting particles, when compared with their predecessors through a number of spectroscopic techniques, are shown to have greatly reduced levels of ‘undesirable’ capping, with a much lower surface oxide level; whilst also maintaining long-term air stability, strong photoluminescence and high yields.

## 1.5 Methods for characterising nanoparticles

**Fourier Transform Infra-red spectroscopy (FTIR)** is a well-known technique that has been used to determine the vibrational structure of molecules. In short, IR absorption due to molecular vibrations (and thus structure) is determined by illuminating a sample with polychromatic light, select wavelengths of which have been omitted. For nanoparticles, FTIR is an important technique to determine the types of molecules present in a sample, and how they are arranged within (or on) the nanoparticle. As with any technique there are limitations, and not all nanoparticles suit FTIR equally. For example, the highly contorted surface of many nanoparticles leads to very complicated spectra that can obscure interesting features. Additionally, scattering effects can skew the collected data.

**Nuclear Magnetic Resonance (NMR)** is another important tool used by researchers to help them understand nanoparticles. By using a magnet to align the spin of atoms (with non-zero spin) and probing them with radio waves, information about the chemical environment of said atoms can be gleaned. This technique is particularly useful at picking up impurities present in a sample, and molecules attached to the surface of a nanoparticle will generally have a distinctive shift in the portion of the molecule that is closest to the surface. However, there are severe problems that are encountered when studying nanoparticles with NMR: First, nanoparticles are seldom diamagnetic, so data can become severely broadened; second, the amount of material required to gather a spectrum can easily make shimming impossible, and third; aggregation can cause nanoparticles to fall out of the measurement region, leading to a loss in concentration and therefore signal strength.

**Photoluminescence spectroscopy (PL)** is a technique used to study the luminescent properties of nanoparticles. By shining monochromatic light at a sample and measuring the spectral response at right angles to the incident light, insights into the fluorescence of nanoparticles can be gleaned. PL can tell researchers a lot about the difference between the surface and core of nanoparticles by studying the response of nanoparticles to external stimuli such as magnetism,<sup>29</sup> or chemicals.<sup>31</sup> For SiNPs this technique is invaluable, as the fluorescence of

## 1.6 Objectives

these particles is still a topic of some debate, and delving into said debate is the purpose of this thesis. As with NMR, sample aggregation and settling will skew the acquired data by scattering the incident light, as well as by decreasing the PL response over time. Luckily, most acquisition times are short enough (10-30 s) that samples will not be unduly affected. However, time-dependent studies must take this into account.

**UV-Vis Spectroscopy** is a powerful technique to gain information on the electronics of molecules. It works in much the same way as IR spectroscopy, with the difference that the electromagnetic region used is in the near-UV to near-IR, spanning the visible spectrum. In the context of nanoparticles it is useful for determining the origin of luminescence, as the particles absorb in their fluorescence region.

**Transmission Electron Microscopy (TEM)** is an imaging technique used to image materials on the nanoscale. Emitted electrons interact with a thin sample of the material being probed, and are collected on a fluorescent plate on the other side of the sample. Due to the low de Broglie wavelength of electrons, much higher resolutions can be achieved compared to conventional optical imaging, to the point of being able to distinguish individual atoms. This resolution is what makes this a useful technique for nanoscience, as it can (for example) give information on the crystallinity of the surface.

**X-Ray Photoelectron Spectroscopy (XPS)** uses X-rays to bombard the surface of a sample. This releases electrons at various kinetic energies depending on their chemical environment, which can be used to resolve the atomic makeup of the surface. Since the penetration depth of X-rays is quite small (~10 nm), this technique gives information on the surface, without this data being swamped by the bulk.

## 1.6 Objectives

This objectives of this thesis are: first, to provide an improved method for the synthesis of SiNPs, giving nanoparticles with lower concentrations of oxide on the surface; and second, to use photoluminescence studies to improve the understanding of the causes of the blue and red luminescence.

## 2 Synthesis of SiNPs

There are many different methods available in the literature for synthesising SiNPs. These include thermal decomposition,<sup>50,51</sup> thermal vapourisation,<sup>52</sup> ion implantation,<sup>53</sup> electrochemical etching,<sup>54</sup> and the chemical decomposition of micelles.<sup>15</sup> Given this vast number of different techniques available for the synthesis, it is necessary to choose a method to use for this work. The two methods used in this work are electrochemical etching, and chemical reduction of micelles, in part due to the relatively simple and low cost of synthesis, and partly due to the existing expertise within the group for these techniques. Both of these techniques produce nanoparticles in a few hours and at room temperature, making them both cheap and easy to produce.

### 2.1 General synthesis of RSiNPs by chemical reduction of micelles

The strength of this technique is its flexibility. The surfactant used to stabilise the micelle can be almost anything, as long as it is a chlorosilane with a good amphiphilicity across the  $\text{SiCl}_4$ /toluene interface. The continuous phase need not be toluene, nor the droplet phase  $\text{SiCl}_4$ . In theory, as long as a stable interface can be formed this technique will produce viable particles. However, since  $\text{SiCl}_4$  micelles in toluene are known to give good results, it is this combination that will be used in this work. It should also be mentioned that all of these reagents react readily with water and atmospheric oxygen, so steps (such as the use of a Schlenk line) must be taken to remove these before performing the synthesis.

This technique works by first forming small stable droplets of a silicon tetrachloride ( $\text{SiCl}_4$ ) in toluene using a trichlorosilane (usually an alkylsilane) as the surface active agent. An equimolar amount of  $\text{SiCl}_4$  and alkylsilane was found to give the narrowest dispersion of nanoparticles. The droplets are broken up using sonication, whereupon a reducing agent (lithium aluminium hydride,  $\text{LiAlH}_4$ ) is added in excess to precipitate the liquid  $\text{SiCl}_4$  into  $\text{Si}_s$  with the alkyl chains from the alkylsilane remaining attached to the surface. The nanoparticles have now been synthesised, but the excess  $\text{LiAlH}_4$  must be quenched. This is done by adding an oxidising agent such as alcohol to precipitate the remaining  $\text{LiAlH}_4$  before working up the dispersion by filtration, evaporation, dispersion in hexane, microfiltration, and further evaporation. Following this procedure yields relatively pure (as determined by FTIR) alkyl-capped silicon nanoparticles (RSiNPs). A schematic (Figure 4) is provided to illustrate this process.

The above procedure does produce RSiNPs, but the addition of alcohol in the quenching step inevitably leads to oxidation, as the alcohol reacts not only with the  $\text{LiAlH}_4$ , but also with vacant (hydrogen-terminated) sites on the RSiNP. This in turn means that the nanoparticles

## 2.1 General synthesis of RSiNPs by chemical reduction of micelles

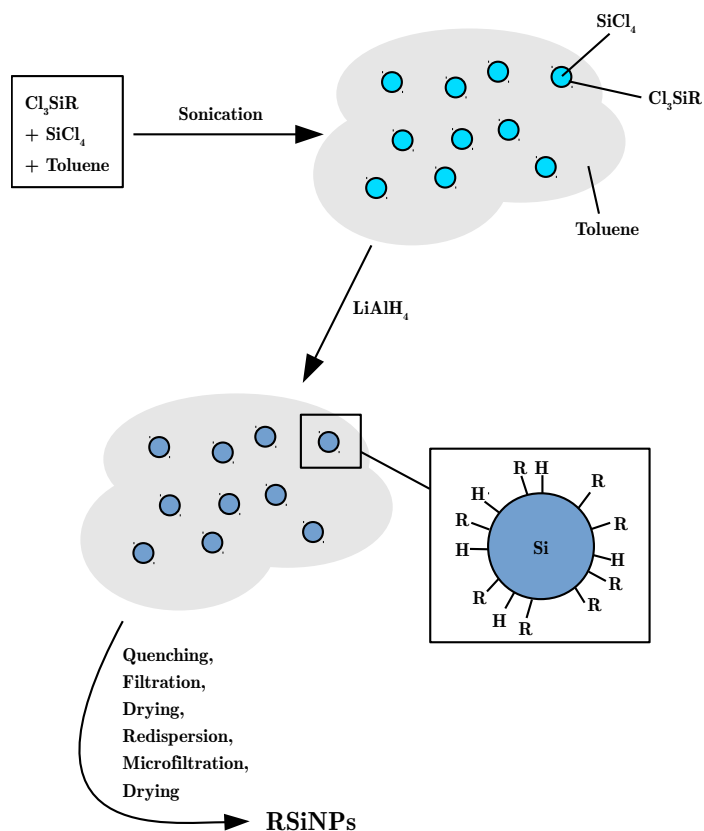


Figure 4: Diagrammatic representation of the synthesis of SiNPs by chemical reduction of micelles.

are more complex (in terms of analysis) and have fewer sites available for further chemistry. The solution to this is to use a quenching agent that will react with  $\text{LiAlH}_4$  but not with the surface of the nanoparticle. The quenching agent chosen for this work was  $\text{CuCl}_2$ , due to its ability to quench  $\text{LiAlH}_4$  and its low reactivity with silicon.  $\text{CuCl}_2$  is also a solid, making it easy to remove the excess after the reaction has finished. The desired differences in surface chemistry between alcohol- and  $\text{CuCl}_2$ -quenched RSiNPs are shown in figure 5.

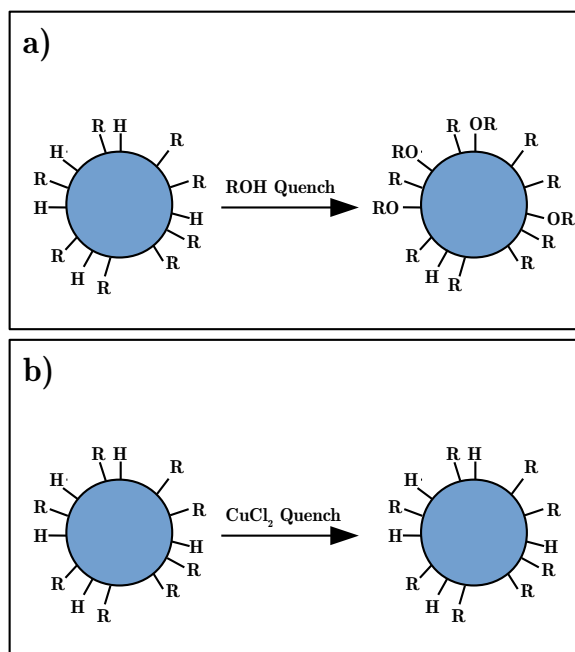


Figure 5: A hypothetical depiction of the changes in surface chemistry as a result of quenching with alcohol (a), or  $\text{CuCl}_2$  (b).

**2.1.1 Synthesis of  $\text{CuCl}_2$ -quenched, dodecyl-capped SiNPs:** Toluene (distilled, 50 ml) was degassed by sonicating under vacuum for five one-minute intervals. The flask containing the toluene was then held under positive nitrogen atmosphere for the duration of the experiment. Trichloro(dodecyl)silane (0.7 mmol, 0.26 ml) was added through a septum fitted to the flask with a syringe, followed by  $\text{SiCl}_4$  (0.7 mmol, 0.1 ml). The mixture was shaken vigorously for one minute before being sonicated for 30 minutes.  $\text{LiAlH}_4$  (1 M in THF, 4 mmol, 4 ml) was then added dropwise to the dispersion, before sonication for two hours. At this stage, the septum was briefly removed to allow for the addition of anhydrous  $\text{CuCl}_2$  (1.5 g). The septum was replaced, the flask flushed with nitrogen, and the mixture shaken briefly before returning to sonication for a further two hours.\* Once the two hours had elapsed, the mixture was filtered twice using a Büchner funnel to remove the off-white precipitate, and the eluted liquid was dried by rotary evaporation to give a thick yellow / orange gel and a small amount of white precipitate. This was then redispersed in 6 ml petroleum ether with the aid of sonication (five minutes), before separation by centrifugation (60 minutes, 7000 rpm). The liquid was decanted, filtered with a PVDF syringe filter ( $0.45 \mu\text{m}$ ), and dried in vacuo to give a pale yellow gel (yield ~100 mg).

**Materials:** Toluene (Fisher, 99.9 %) dried over sodium wire; methanol (Sigma-Aldrich, 99.8 %); hexanes (Fisher, 99.9 %); lithium aluminium hydride solution (Fisher, 1 M in THF);

\*NB: small amounts of silane gas may be evolved at this stage

## 2.1 General synthesis of RSiNPs by chemical reduction of micelles

silicontetrachloride (Sigma-Aldrich, 99 %); trichloro(hexyl)silane (Sigma-Aldrich, 97 %) stored under N<sub>2</sub>; trichloro(octyl)silane (Sigma-Aldrich, 97 %) stored under N<sub>2</sub>; trichloro(dodecyl)silane (Sigma-Aldrich, 95 %) stored under N<sub>2</sub>; and anhydrous copper (II) chloride (Sigma-Aldrich, 98 %).

### 2.1.2 Machine specifications for characterisation

**FTIR** – Fourier transformed infrared spectra were collected using a Perkin-90 Elmer Spectrum 100 ATR FTIR spectrometer. The pure gel product was placed on the crystal and measured versus a background spectrum of the clean crystal.

**NMR** - Proton nuclear magnetic resonance measurements of samples dissolved in CDCl<sub>3</sub> were taken using a Bruker 500 MHz NMR spectrometer. Samples were scanned 16 times.

**PL** - Photoluminescence spectra were taken for samples dissolved in toluene in a quartz cuvette (10 mm × 10 mm), using a Perkin-Elmer LS55 spectrophotometer with emission bandwidth of 10 nm, and excitation bandwidth set to 20 nm. The wavelength cut-off was set to 390 nm. In each case, the excitation wavelength used in the 65 emission spectrum corresponds to the excitation spectrum maximum, and vice versa, iterating to get the optimum result.

**TEM** - High-resolution transmission electron microscopy studies were performed with a Philips CM200 FEGTEM microscope. Atomic number contrast (Z-contrast) Scanning TEM (STEM) imaging was performed on a Nion UltraSTEM 100, operated at 100 kV using a cold field emission electron source, and a corrector capable of neutralizing aberrations up to fifth order. TEM samples were prepared by dropcast SiNPs solution onto graphene substrate. The solvent was evaporated and TEM micrographs were typically taken at different spots of each grid. Samples were baked at 135°C for approximately 7 h in a turbo backed vacuum oven prior to STEM imaging to reduce contamination.

**XPS** - X-ray photoelectron spectroscopy measurements were taken using a K-Alpha XPS instrument (Thermo Scientific, East Grinstead, UK). A monochromatic Al K $\alpha$  X-ray source (1486.6 eV) was used with a spot size of 400  $\mu$ m diameter. A pass energy of 200 eV and step size of 0.4 eV was used for survey spectra, and a pass energy of 40 eV and step size of 0.1 eV was used for high-resolution spectra. A few drops of dry SiNP gel were cast onto a clean gold substrate. This was transferred into a load-lock attached to an ultra-high vacuum (UHV) chamber. For all photoemission spectra, the binding energies (BEs) are referred to the Au4f

line, as measured on a gold foil in direct electrical contact with the sample, which lies at BE of 87.4 eV.

**Quantum yield (QY)** - The quantum yield of the alkyl-capped SiNPs was calculated with the Eq. 2:

$$Q = Q_R \left( \frac{Grad}{Grad_R} \right) \left( \frac{\eta^2}{\eta_R^2} \right) \quad (2)$$

where Q is the quantum yield and Grad is the gradient from a plot of integrated fluorescence intensity against absorbance. The subscript R refers to the reference fluorophore of known quantum yield. Here Quinine Sulphate was used as reference, which has a quantum yield of 54.6 % when dissolved in 1 N H<sub>2</sub>SO<sub>4</sub>. 1 N (0.5 M) H<sub>2</sub>SO<sub>4</sub> had a refractive index  $\eta_R$  of 1.346, while the refractive index  $\eta$  of hexane was 1.3749.

## 2.2 General synthesis of HSiNPs by electrochemical etching

This technique, while employing hydrogen fluoride and high current, is a relatively fast way of obtaining uncapped SiNPs (i.e. capped with very labile hydrogen atoms), usually taking no more than four hours. These SiNPs can also be coated in a variety of ligands. For example, Ahire *et al* (2012) used H<sub>2</sub>PtCl<sub>6</sub> to catalyse the reaction between hydrogen-capped SiNPs and allylamine, attaching the ligand by the alkene end to give a SiNP with solution-facing amine groups.<sup>13</sup> Another strength of this technique is that the size of the particles can be controlled by altering the current density and etching time, as shown by Coxon *et al* (2011).<sup>24</sup>

The nanoparticles are formed by running a high current density through a solution of HF and EtOH, using silicon wafer as the anode. This etches the surface of the wafer, producing H<sub>2</sub>SiF<sub>6</sub> and evolving H<sub>2</sub> gas. The SiNPs are produced in the nanostructure of the porous part of the wafer, which is smoothed and passivated by the HF to give hydrogen-capped SiNPs. The wafer is then removed from the solution and dried under vacuum. Once dry, toluene is added to the wafer and it is sonicated to disperse the HSiNPs into solution. The nanoparticle-laden toluene can then be decanted and used as-is.

**2.2.1 Synthesis of hydrogen-capped SiNPs:** Silicon wafer was cut into squares (~8×8 mm) using a diamond pen and the chips were stored covered in the etching solution for at least half an hour to remove surface oxide. The etching solution was made up of a 1:1 mixture of HF (aqueous, 48%) and ethanol. One chip was then placed into the etching cell<sup>†</sup> (see figure 6 for

<sup>†</sup>The cell must be assembled gently enough that the wafer does not crack, but still firmly enough that HF cannot leak out. Failure of either of these requirements leads to an increased potential difference across the cell and poor nanoparticle formation.

## 2.2 General synthesis of HSiNPs by electrochemical etching

diagram of cell), the cell was filled with fresh etching solution, and etching was performed for 10 minutes at a current density of  $400 \text{ mAcm}^{-2}$  with a constant current source. Once finished, the etching solution was discarded into  $\text{CaCO}_3$  and the chip was quickly transferred to a flask attached to a Schlenk line. The wafer was then placed under vacuum to dry for a minimum of two hours.

Due to the low NP yield from an individual chip, it was customary to etch several chips in succession and add them to the same flask. The chips already in the flask were kept under vacuum, and the final drying time was measured from the addition of the final chip.

Once dry, toluene was added to the flask (2.5 ml per chip) and the flask was swirled under sonication for 30 s. The cloudy, orange-tinted toluene was then decanted.

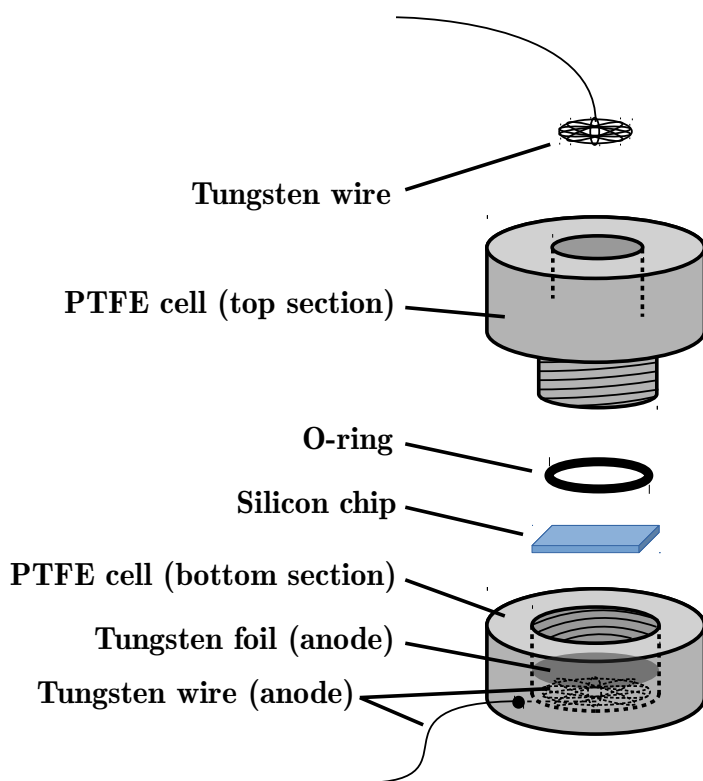


Figure 6: Electrochemical etching cell used for production of hydrogen-capped SiNPs

**Materials:** Toluene (Fisher, 99.9%) dried over sodium wire; Boron doped p-Si (1 0 0) silicon wafer (Compart Technology, Peterborough, UK), resistivity  $10 \Omega \text{cm}^{-1}$ ; Hydrogen fluoride (Sigma-Aldrich, 48% in aqueous solution); Ethanol (Fisher, 99.6%).

**Etching cell materials:** Cell (machined PTFE); O-ring (Viton, teflon-coated); Tungsten wire (Sigma-Aldrich, 0.5 mm). Tungsten foil (Sigma-Aldrich, 0.05 mm). Constant current source (Keithley Source Meter 2061).

### 3 CuCl<sub>2</sub>-quenched SiNPs

The aim of this work is to optimise the method detailed in previous publication in order to maximise alkyl capping and minimise the remaining Si–H functionality, and also to eliminate the use of alcohol to quench the reaction in order to avoid the unintentional resulting particle oxidation, particularly in light of the fact that any remaining Si–H functionality after the formation of alkoxy groups has shown high levels of stability versus atmospheric oxygen, when part of the otherwise highly passivated SiNP system.<sup>15</sup> Equally, this chapter will provide a detailed insight into the nature of the particles produced, with characterisation via a number of spectroscopic techniques.

The purpose of the first stage of this work was to improve upon and optimise SiNP synthesis, based on the previously reported method.<sup>15</sup> Figures 7, 8 and 9 shows various techniques designed to elucidate the nature of the nanoparticles synthesised using the optimised technique. The FTIR spectrum in figure 7 shows strong C–H absorption at 2922 and 2852 cm<sup>-1</sup> and Si–C absorption at 1464 and 1260 cm<sup>-1</sup>, indicating functionalization of the surface with the organic ligands. The weak silicon oxide peaks at 1094 and 1018 cm<sup>-1</sup>, coupled with the presence of significant silicon hydride peaks at 2148 cm<sup>-1</sup> indicate relatively low levels of surface oxidation and good protection of the surface due to the organic ligands. Despite obvious limitations to the use of NMR for study of colloidal systems, some useful information can still be obtained. In this case, the <sup>1</sup>H-NMR spectrum shown in figure 8 contains a characteristic Si–CH<sub>2</sub> peak at 0.5 ppm, as well as CH<sub>2</sub> peaks at 1.2 ppm and a CH<sub>3</sub> peak at 0.8 ppm. A strong peak at 3.45 ppm is related to Si–O–CH<sub>3</sub>. The XPS spectrum in figure 9 shows the presence of Si, O and C, but no residual Cu or Cl from the reducing agent. It should be noted that the relatively weak oxygen line present in the sample is likely due to X-ray-induced oxidation.<sup>24,55</sup> An image of the blue luminescence observed in these SiNPs under UV light (365 nm) can be found in figure 10. It is worth noting that samples left uncovered in a cupboard for a period of 1 week show no change in FTIR peak intensities. This indicates high particle stability and resistance to any form of degradation or further oxidation due to exposure to atmosphere, contrary to suggestions made by Wang *et al* (2011).<sup>47</sup>

The data has shown significantly reduced Si–O peaks compared to alcohol-quenched SiNPs, whilst maintaining and improving the remainder of the particle surface structure, including the retention of minimal Si–H surface functionality. This indicates high desirable surface coverage has been achieved, and that the particles are not subject to oxidative degradation in air. The particles also demonstrate notable optical properties. Figures 11 and 12 show the PL excitation and emission spectra of the synthesised SiNPs at 345 nm, and the UV–Vis spectrum of the same sample, respectively. These spectra are typical of SiNPs made using the micelle technique,<sup>15,47</sup> showing a strong blue luminescence and a lack of red lumi-

nescence. This lack of red luminescence may be due to the lack of hydroxide present on the surface of the nanoparticles, as these RSiNPs are synthesised in a dry, waterless environment.

Photoluminescence quantum yields, see figure 13, of the alkyl-capped SiNPs in hexane were obtained using quinine sulphate (QY = 54.6 %) as a reference emitter (Xiong et al. 2006). A solution of SiNPs in hexane with absorbances between 0.1 and 0.01 was prepared, and the gradient of the plot of integrated fluorescence intensity against absorbance was found. The quantum yield of alkyl-terminated SiNPs was found to be at approximately 14 % with an excitation wavelength at 340 nm. The observed QY value in hexane is comparable to values of QY for SiNPs reported in the literature, which range from 2 to 18 %.<sup>56,57</sup> The lack of PL stability of nanostructured silicon is one of the major barriers to the commercial application.<sup>57</sup> To investigate the PL stability in hexane further, time-dependent PL spectra of alkyl-terminated SiNPs were measured by monitoring the emission using an excitation wavelength of 340 nm, as seen in figure 14. In the results shown in this figure, it can be seen that the PL from dodecyl-capped SiNPs decreases over 3 weeks due to aggregation in the sample, but is still strong (about 77 % of initial PL intensity). This is a much better product than other semiconductor QDs, which implies the monolayer formed is robust towards oxidation over long periods of time. A couple of examples of the nanoparticles as seen using aberration-corrected STEM can be found in figure 15. This image shows that the nanoparticles are reasonably monodisperse, with no very large or very small particles present. Analysis of this and similar images gave a mean particle size of about 5 nm. The inset image in figure 15 shows the crystalline nature of these nanoparticles. It should be noted that the drying process necessary for STEM imaging (i.e. heating to 135°C for 7 h) may have annealed the nanoparticles, giving the neatly arranged atoms seen in the inset in figure 15. However, since the nanoparticles were distant enough not to aggregate under heating, the inset is still a good indicator of the size of the nanoparticles.

As can be seen from figure 16, the SiNPs quenched by MeOH show strong Si–O–C peaks at 1094 and 1018  $\text{cm}^{-1}$ , peaks which are hardly visible in the sample quenched with  $\text{CuCl}_2$ . This suggests that the  $\text{CuCl}_2$ -quenched SiNPs are not significantly oxidized. Indeed, the  $\text{CuCl}_2$  SiNPs still show Si–H functionality but when compared to that of EtOH-quenched SiNPs prior to optimisation, there is a significant reduction in the intensity of the Si–H peak.

The fact that these nanoparticles contain very little oxide, yet are still brightly luminescent suggests that even if one or several components in the spectrum are due to silica - as suggested by Coxon *et al* (2011)<sup>24</sup> - there are still several components in the blue region that are still not explained. These low-oxide and reduced-hydride SiNPs are an excellent starting point to fully explaining the behaviour of these nanoparticles, as their elemental simplicity reduce the effects of these parameters. The evidence provided by FTIR shows that using copper chloride to quench excess  $\text{LiAlH}_4$  lowers both the level of oxide and the level of hydride

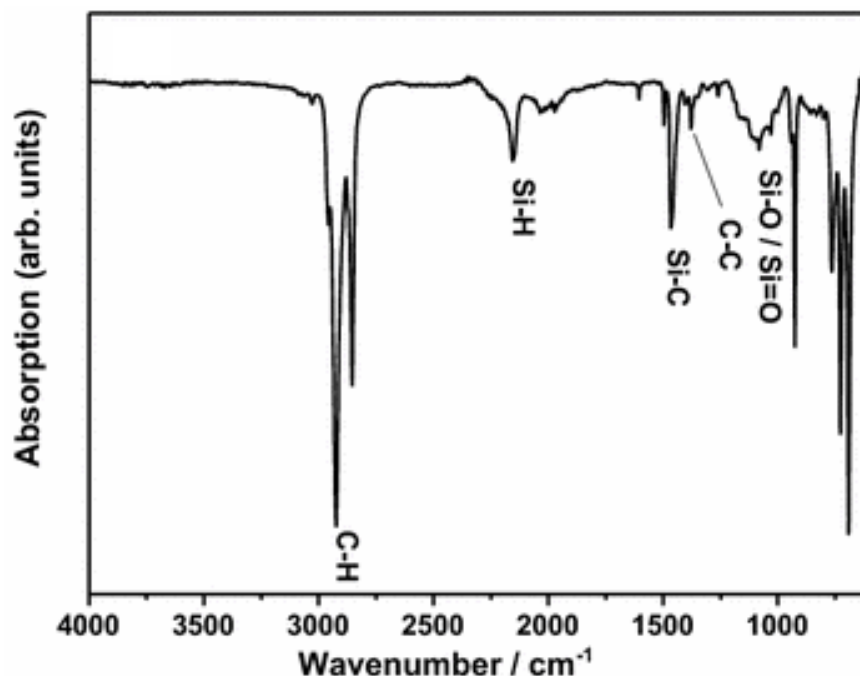


Figure 7: FTIR spectrum for  $\text{CuCl}_2$ -quenched, dodecyl-capped SiNPs.

on the SiNPs when compared to previous methods using short-chained alcohols.<sup>15</sup> This is significant, as not only are the samples more chemically pure, but there is a lack of methoxy and ethoxy groups present on the surface of the particles, which simplifies further synthesis, as complications due to these groups can be discounted. Indeed, the evidence presented here indicates that there may be enough silicon hydride left on the surface to be considered viable reactive sites for further chemistry, although reagents would have to be more reactive than molecular oxygen. The origin of PL in SiNPs is a topic of great debate in the literature, and is complicated by the observation of both direct and indirect band gap transitions.<sup>58</sup> Discreet orange and blue luminescence - rather than a spectrum of colours - are observed with SiNPs, with shifts to other wavelengths proving difficult to achieve.<sup>31</sup> Theories as to the origin of this phenomenon have been attributed to particle size and surface states,<sup>59</sup> and also to particle ligands and surface oxidation.<sup>30</sup> In the work of Vial *et al* (1992),<sup>51</sup> the quenching of orange luminescence is attributed to the addition of a nitrogen containing surfactant into a SiNP system. The resulting system then begins to show blue luminescence, a phenomenon which is attributed to sites of oxidation on the particles surfaces. These conclusions are made by virtue of a colour change upon titration of a nitrogen containing surfactant in air into a sample of SiNPs, with the observation of the associated orange to blue colour change. Although this observation is justified, the work presented here shows no orange luminescence, despite there being no presence of any nitrogen containing surfactant or compound, and no nitrogen being present on the sample surface (see above FTIR spectra and the XPS surface elemental analysis

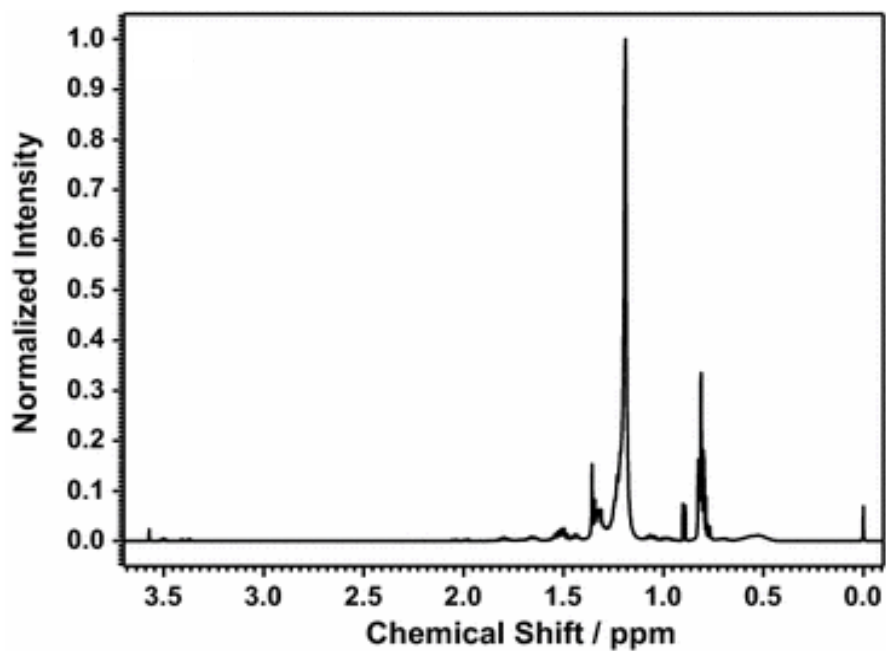


Figure 8: NMR spectrum for  $\text{CuCl}_2$ -quenched, dodecyl-capped SiNPs.

shown in Figures 7 and 9). Equally, a strong blue luminescence can be seen in samples both with high and also comparatively negligible surface oxidation from the two synthesis methods presented. This implies a more complex system than the production of peaks from a single class of ligands.

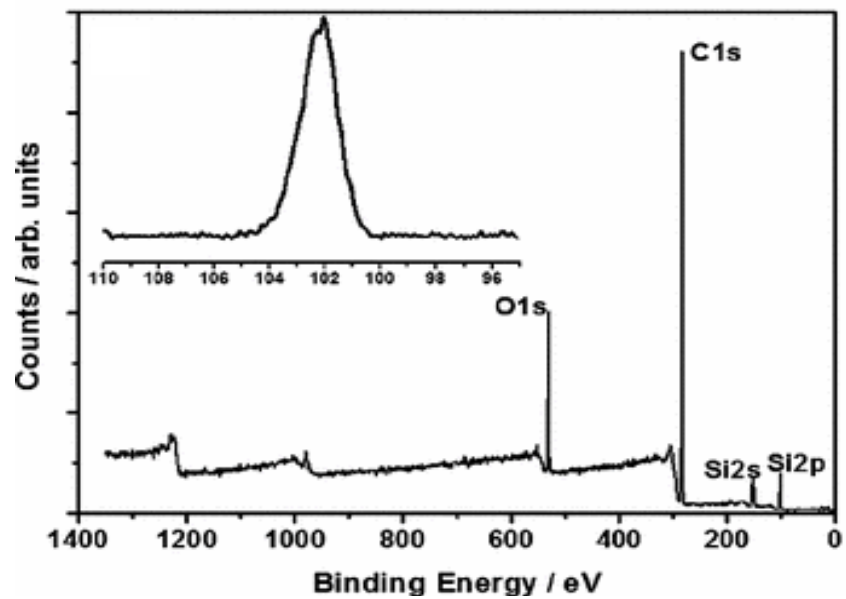


Figure 9: XPS spectrum for  $\text{CuCl}_2$ -quenched, dodecyl-capped SiNPs. The inset is the high-resolution Si2p peak.

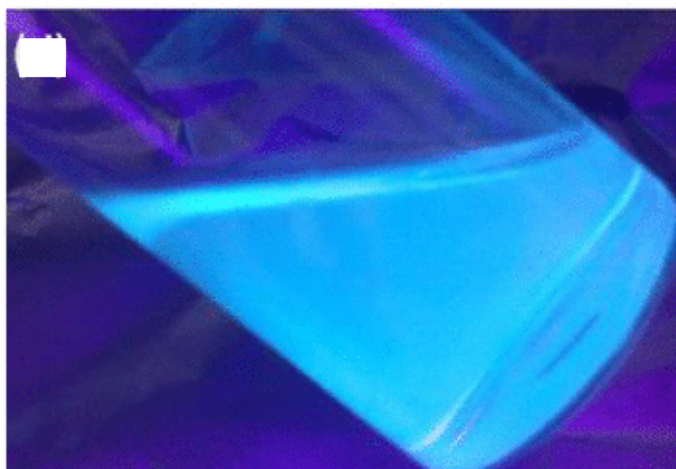


Figure 10: Image of  $\text{CuCl}_2$ -quenched, dodecyl-capped SiNPs under UV irradiation at 365 nm.

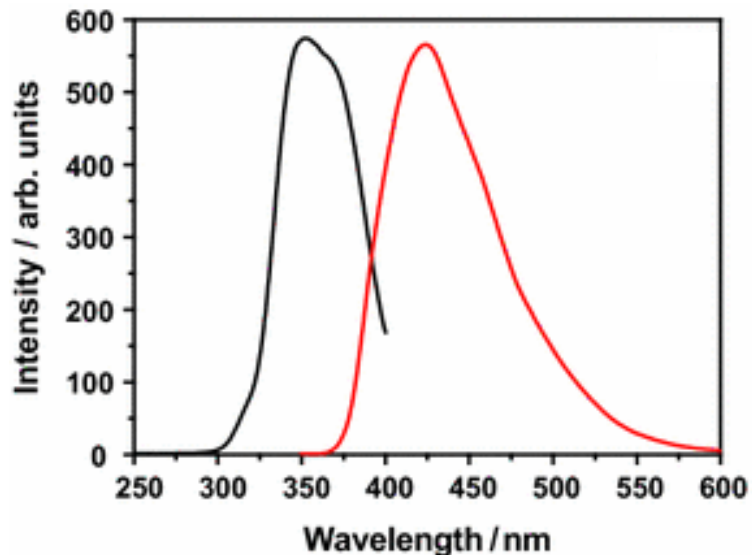


Figure 11: PL spectrum of  $\text{CuCl}_2$ -quenched, dodecyl-capped SiNPs: the black line is the excitation spectrum measured as the response of the emission at 420 nm, while the red line is the emission spectrum with an excitation wavelength of 345 nm.

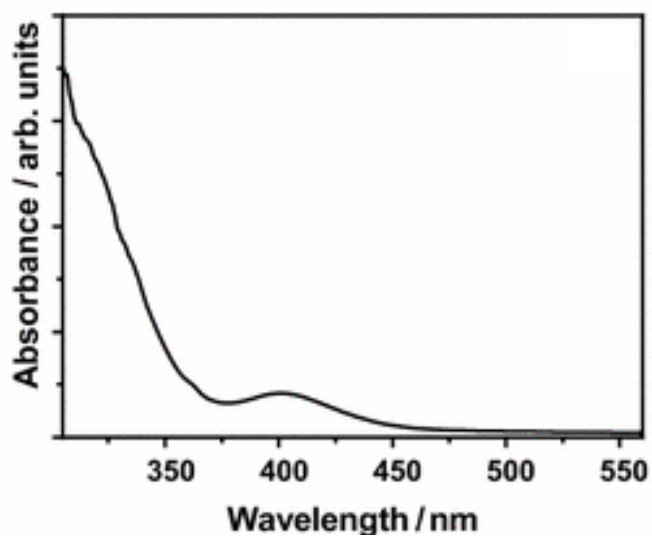


Figure 12: UV-Vis spectrum of  $\text{CuCl}_2$ -quenched, dodecyl-capped SiNPs.

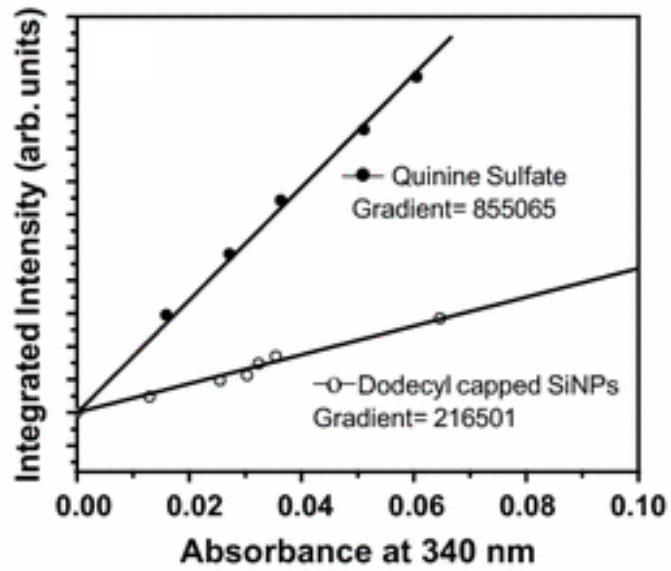


Figure 13: Integrated PL intensity against absorbance for diluted dodecyl-capped SiNPs in hexane and quinine sulphate in 1 M H<sub>2</sub>SO<sub>4</sub> solution for QY measurement, collected under the excitation at 340 nm and ambient conditions.

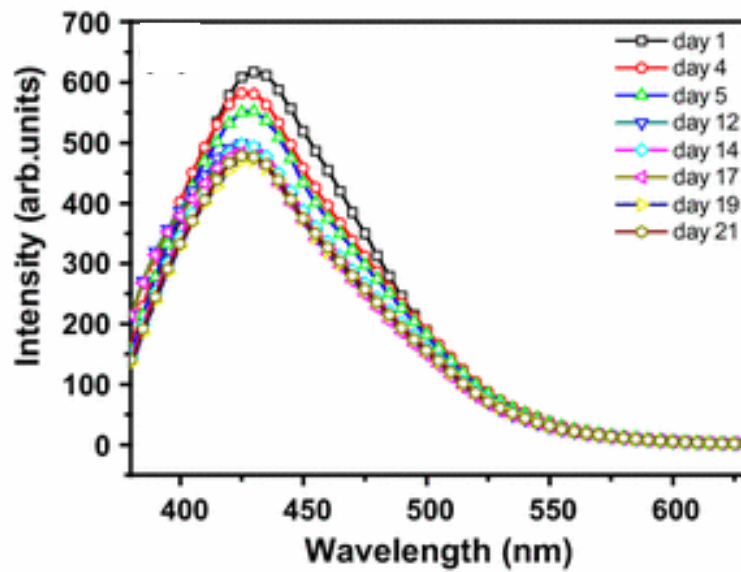


Figure 14: PL decay spectra monitored over 21 days with excitation wavelength of 340 nm.

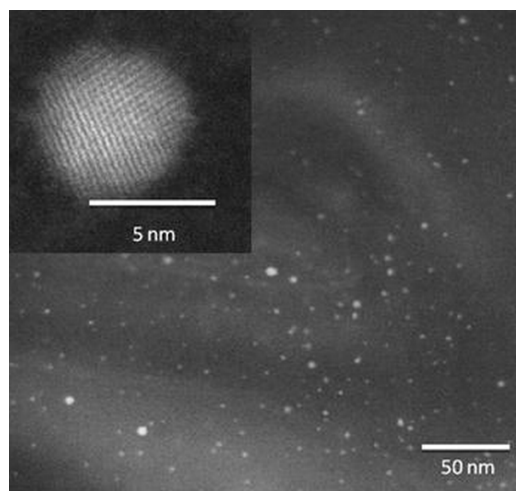


Figure 15: Aberration-corrected STEM images of the SiNPs made using the inversed micellar method quenched through introduction of  $\text{CuCl}_2$ . Inset is a high-resolution TEM image with visible crystal nature of a SiNP.

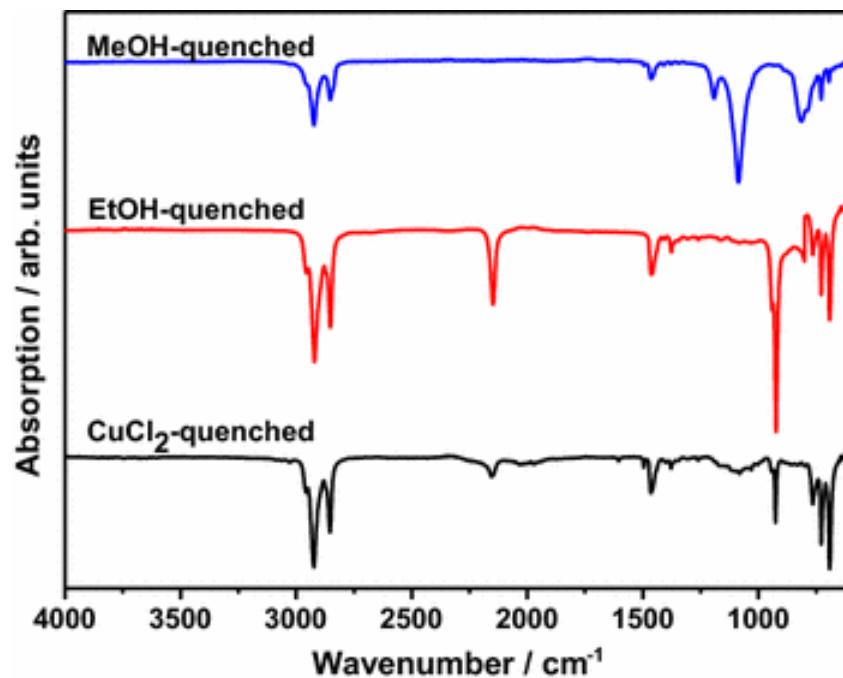


Figure 16: FTIR comparison of MeOH-quenched SiNPs (top), EtOH-quenched (middle), and  $\text{CuCl}_2$ -quenched, dodecyl-capped SiNPs (bottom)

## 4 Photoluminescence of SiNPs

In order to probe the optical properties of SiNPs, the behaviour of said properties in different environments must be investigated. For example, process A with intensity  $a$  is negatively affected by application of a certain chemical species to the solution, while process B with intensity  $b$  is positively affected. If the changes to A and B are related by a first-order equation, this implies that A and B are indirectly affected by each other (such as shielding). If a certain fluorescent peak decreases (in intensity) upon application of an external stimulus, this implies that the process is being hindered. If a different peak increases in intensity under the same conditions, it could be that the first process is shielding the second, and the suppression of the peak has increased the relative incident intensity. It is also possible that the second peak increases because the conditions are such that there are more active sites for that specific process to occur. To bring these hypotheticals into the real world, the application of, say, nitrogen-containing compounds to a suspension of SiNPs (as shown by Dasog *et al*, 2013)<sup>30</sup> causes a decrease in the red luminescence and an increase in the blue, but whether this increase is direct or indirect is difficult to determine. However, it is reasonable to assume from the total change of the blue luminescence that this process is directly affected by the nitrogen. Therefore, a similar experiment using a variety of oxygen-containing chemicals was performed, as well as a brief investigation into the effect that a concerted effort to remove oxygen from the synthetic process may have on the final luminescence.

### 4.1 Photoluminescence characterisation of HSiNPs

PL spectra of HSiNPs synthesised by electrochemical etching were obtained under different chemical conditions. The toluene used to disperse the NPs was either used directly as received from the manufacturer (neat), distilled (dry), or distilled and then degassed to remove dissolved oxygen. Chemicals used to probe the PL response of the NPs were methanol, ethanol, isopropanol, phenol, and tertbutylphenol. A few drops of these chemicals were added directly to the quartz cuvette used for gathering the PL spectra and shaken vigorously before immediately measuring the sample. The PL was also measured as a function of time, to give information on the reaction rate of the SiNPs with the added chemicals.

The PL spectra obtained were fitted to a set of gaussian functions, with the number of Gaussians being chosen to give the best real fit. The overall fitting equation for the intensity  $I$  is given by:

$$I = \sum i_n e^{-\frac{(x-p_n)^2}{2c_n^2}} \quad (3)$$

Where  $i$  is the height of the peak at its maximum (i.e. the intensity of the peak),  $p$  is the

#### 4.1 Photoluminescence characterisation of HSiNPs

position of the peak at its maximum, and  $c$  is the width at half maximum.  $n$  was typically chosen to be 4 or 5 depending on the goodness of fit. Figure 17 shows an example of the PL response of a sample of SiNPs in toluene, with the corresponding fitted Gaussians, as well as showing that the synthesis technique used does indeed yield luminescent SiNPs.

In order to account for differences in concentration from sample to sample, as well as the odd occasion where bandwidths had to be modified to obtain a reading, the PL spectra were normalised by one of the peaks resulting from fitting. This was chosen to be the smaller peak in the 470-500 nm region as it was almost always present, varied little with time, and was not affected in any significant way by the conditions that the HSiNPs were subjected to. The downside to this approach is that any information contained in this peak is lost.

First, the difference in PL when the SiNPs were dispersed in toluene of different purity was investigated. The PL for these is shown in figure 18a. Note that while the red peak (at ~630 nm) decreases when water is removed, and then decreases further as dissolved oxygen is removed, the blue peak (at ~415 nm) shows a large increase in the distilled sample, but then drops down to a similar level as the neat toluene when the sample is degassed. Note also the significant blueshift in the distilled and degassed samples as compared to the unmodified sample. The same comparison, but with ethanol added to the samples can be found in figure 18b. Here, the PL for the neat and distilled samples are fairly similar to those of figure 18a, with the exception that the sample made with neat toluene is already blueshifted, and the red peak is suppressed down to a level similar to that of the sample made with distilled toluene. The sample made with toluene that was both distilled and degassed, however, is very different with a more intense red peak and a vastly increased blue peak.

A simpler way of visualising the difference between samples is to condense the PL spectra into coordinates of their peak maxima. This gives a simplified version of the spectra, showing only the most pertinent data. An example of this is given in figure 19, where the points on the graph correspond to the lines by colour. It can be seen in this figure that the intensities of the peaks in the blue region (400-500 nm) are convoluted, as they all lie beneath their corresponding line. However, the red peak (~630 nm) is superimposed on the line, as there are no other components of the fitting in that region.

Figure 20 groups together the samples by various criteria; with 20a for HSiNPs dispersed in neat toluene, 20b for HSiNPs dispersed in distilled toluene, and 20c for HSiNPs dispersed in dry and degassed toluene. Figure 20d groups the samples in neat toluene with added aromatic compounds.

As can be seen from figure 20a, the intensity of the blue region increases with increasing chain length of alcohol, with methanol showing the smallest increase and isopropanol showing the largest. The red peak initially shows the opposite trend, with the control showing a greater intensity than either methanol or ethanol, but with isopropanol showing a very large increase.

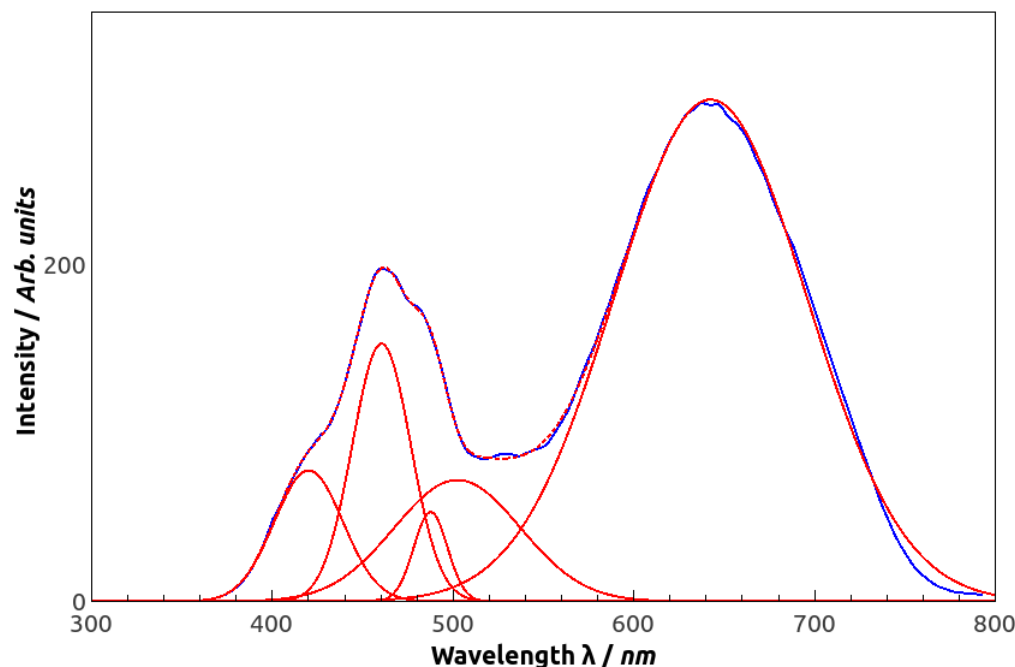


Figure 17: Example of the Photoluminescence of SiNPs at an excitation wavelength of 340 nm, with a superimposed multiple Gaussian fit. The blue line is the raw data, the red lines are the component Gaussians that together make up the fitting function, and the dotted red line is the resulting fit.  $R^2 = 0.998$

For figure 20b, the opposite trend is seen in the blue, with the intensities dropping slightly from the control to methanol and ethanol. Very little change is seen in the red peak region in this graph, with a small increase in intensity between the control and methanol, and a decrease in intensity between methanol and ethanol. Figure 20c shows a very large increase in intensity between the control and the sample with added ethanol on all points, with the largest increase occurring in the blue region. Finally figure 20d shows an increase in the blue and a small increase in the red.

In order to get an idea of the shifts that the peaks undergo under varying conditions, the wavelengths and intensities of the fitted peaks ( $p$  and  $i$  from equation 3) have been summarised in table 1. The wavelengths are grouped in such a way that it is possible to distinguish between different peaks, and have been labelled  $\alpha$  to  $\zeta$  in order of ascending wavelength. From table 1 it can be seen that the ' $\alpha$ ' peak in the 400-410 nm region is only present in the dry and degassed samples, and in the neat samples once the added molecule is large enough (i.e. ethanol and up). It is never present in the distilled samples. There is little variation in wavelength for this peak, while there is a large difference in intensity, with the ethanol sample showing an intensity seven times greater than the toluene sample.

The two peaks ' $\beta$ ' and ' $\gamma$ ' in the 420-440 nm and 451-740 nm regions (respectively) are

	$\alpha$	$\beta$	$\gamma$	$\delta$	$\epsilon$	$\zeta$
Toluene (neat)		424 / 0.91	461 / 1.81	487 / 0.87	510 / 0.82	643 / 3.31
Toluene (dry)		435 / 5.63	464 / 0.33	486 / 0.96	499 / 1.79	645 / 1.32
Toluene (dry and degassed)	402 / 1.49	430 / 1.75			469 / 0.91	633 / 0.31
Methanol (neat)		429 / 3.72	462 / 3.98	487 / 2.25	510 / 2.46	635 / 2.93
Methanol (dry)		431 / 4.33	464 / 2.28		500 / 1.00	655 / 0.60
Ethanol (neat)	408 / 3.21		457 / 2.91	487 / 0.98	499 / 1.07	649 / 1.66
Ethanol (dry)		426 / 4.87	459 / 5.33	488 / 1.04	497 / 2.05	626 / 1.82
Ethanol (dry and degassed)	405 / 10.66	435 / 20.00		484 / 1.26	486 / 8.05	637 / 6.22
Isopropanol (neat)	405 / 6.27		455 / 6.39	488 / 1.05	530 / 2.59	624 / 24.87
Phenol (neat)	402 / 2.20	436 / 2.38			478 / 0.87	630 / 5.00
Tertbutylphenol (neat)	408 / 2.08	457 / 2.54			473 / 1.00	638 / 2.34

Table 1: Initial peak positions  $p$  (nm) /  $i$  (arb. units) as a result of fitting using equation 3. Emphasis indicates the peak used for normalisation.

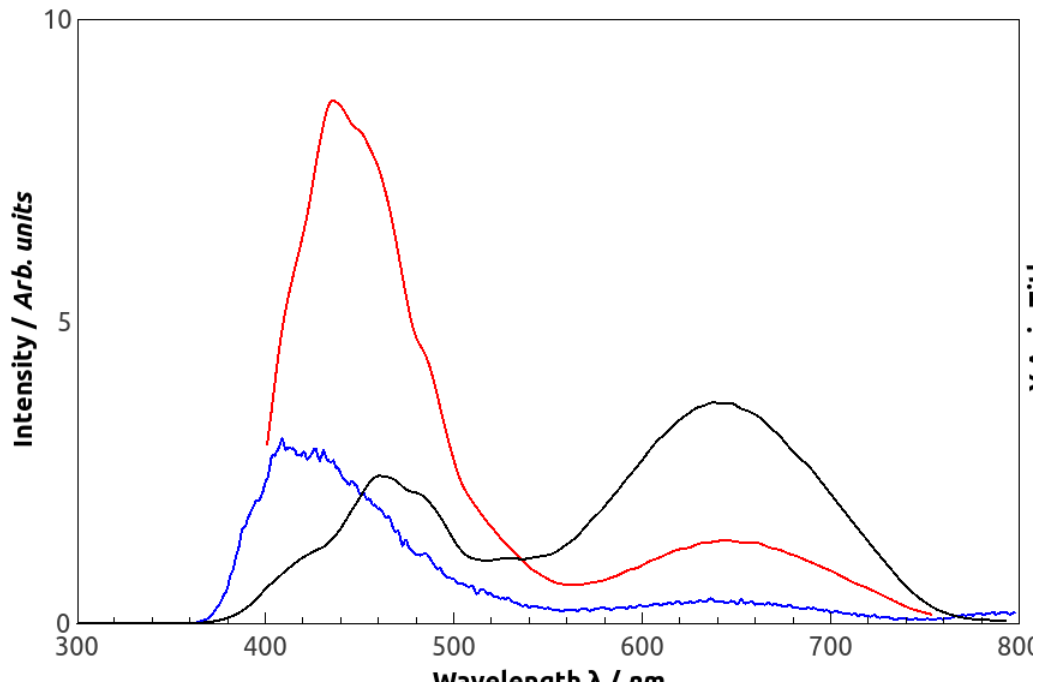
almost always present, with some absences only in the ethanol, isopropanol, and aromatic samples. For the 'dry and degassed' ethanol sample, it is very likely that the very intense peak at 435 nm ( $\beta$ ) has hidden the neighbouring  $\gamma$  peak from being picked up by the fitting function.

The two peaks (' $\delta$ ' and ' $\epsilon$ ') in the 481-500 nm region would be very difficult to distinguish, were it not for the fact that their widths differ by a large amount.  $\delta$  is very narrow, while  $\epsilon$  is very broad. These are the peaks that were used to normalise against, using  $\epsilon$  when the  $\delta$  peak was missing. As with the  $\beta$  peak in the case of dry and degassed ethanol, the four missing peaks in  $\delta$  have likely been misattributed to  $\epsilon$  by the fitting function.

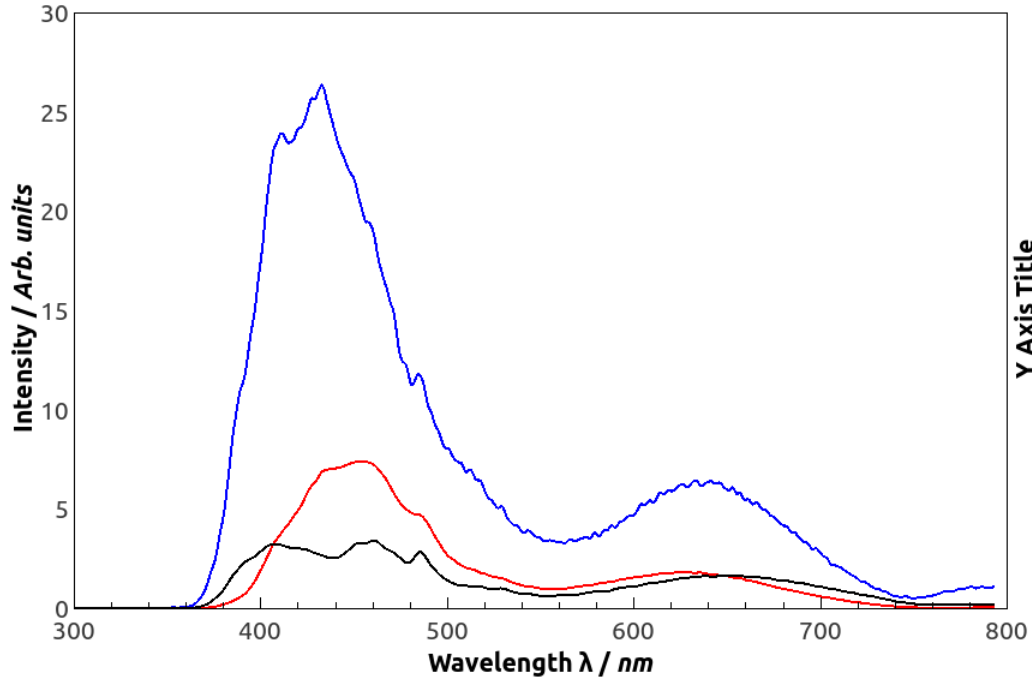
The final peak, ' $\zeta$ ', in the 620-660 nm region, exists in all samples, although the positions and intensities vary greatly. For the 'neat' samples, the peaks are generally blueshifted upon application of the oxygen-containing compound when compared to the control. The exception here is the sample containing ethanol, which displays a small redshift. Equally, there is a large variation in intensity between samples, with a very high intensity in the isopropanol sample.

This implies that oxygen is the cause of luminescence, with dioxygen being the cause of the blue luminescence and hydroxide being the cause of the red. The addition of alcohols shows that the luminescence can be controlled by varying the electronegativity on the oxygen.

#### 4.1 Photoluminescence characterisation of HSiNPs



(a) PL comparison of HSiNPs dispersed in neat toluene (black line), distilled toluene (red line), and toluene that had been both distilled and then degassed (blue line).



(b) PL comparison of HSiNPs with ethanol post-added, dispersed in neat toluene (black line), distilled toluene (red line), and toluene that had been both distilled and then degassed (blue line).

Figure 18: PL spectra of HSiNPs dispersed in toluene, comparing levels of oxygen and water in toluene (a), and levels of oxygen and water with added ethanol (b).

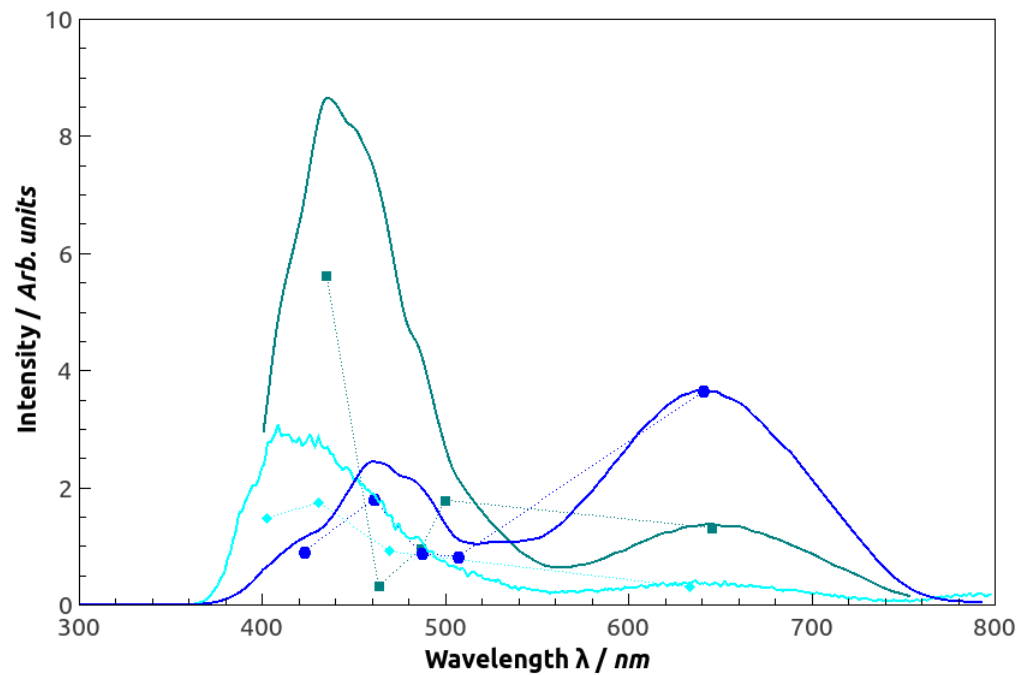
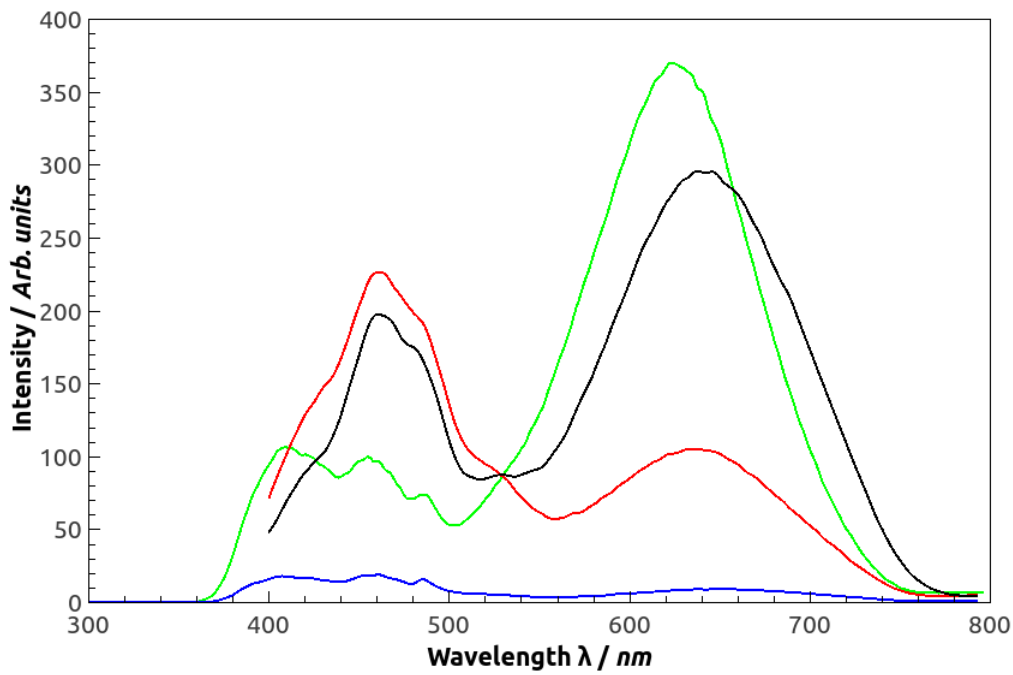
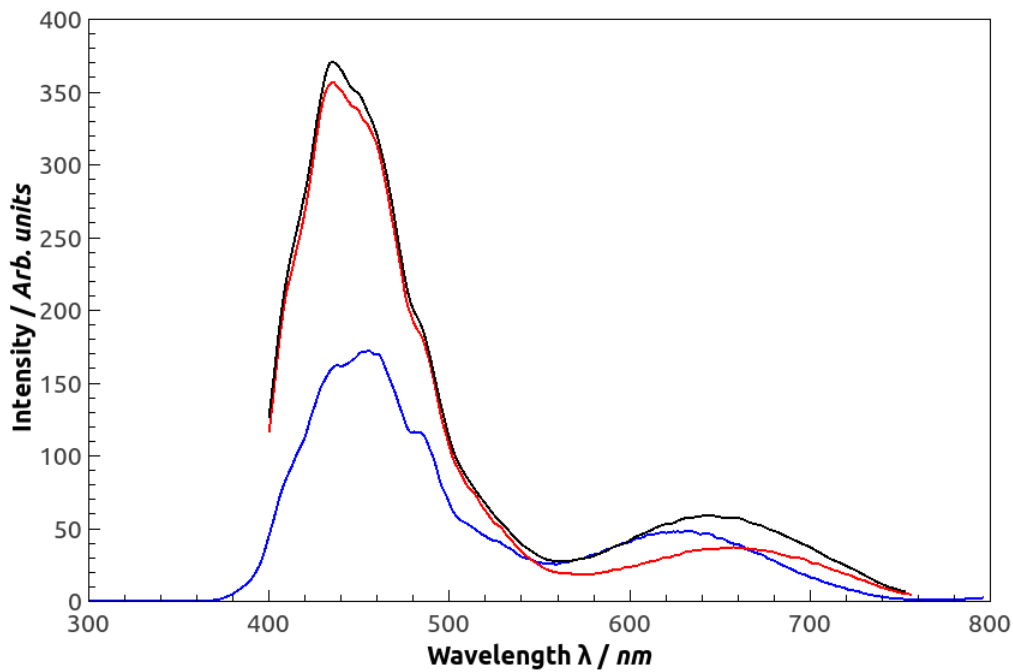


Figure 19: PL comparison of HSiNPs dispersed in toluene, with the maxima of the fitted peaks superimposed over the top. The three curves are neat toluene (blue line, blue dots), distilled toluene (dark cyan line, dark cyan squares), and toluene that had been both distilled and then degassed (cyan line, cyan diamonds). The dotted lines are for ease of visualisation only.

#### 4.1 Photoluminescence characterisation of HSiNPs

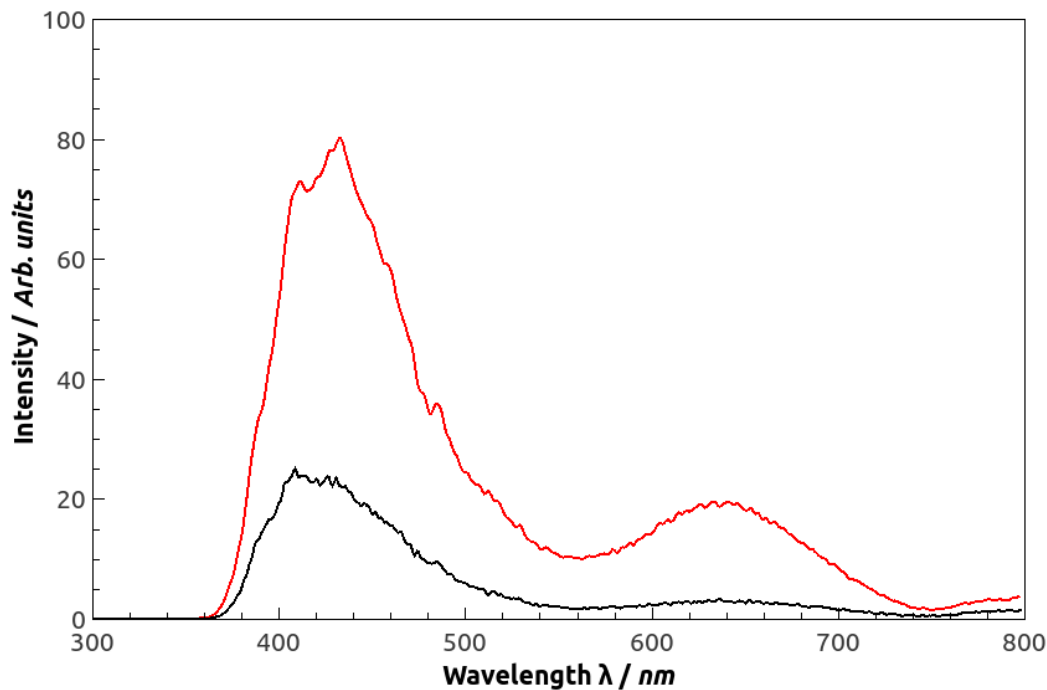


(a) PL spectra for samples of HSiNPs dispersed in neat toluene, with added alcohols. Control (black line), methanol (red line), ethanol (blue line), and isopropanol (green line).

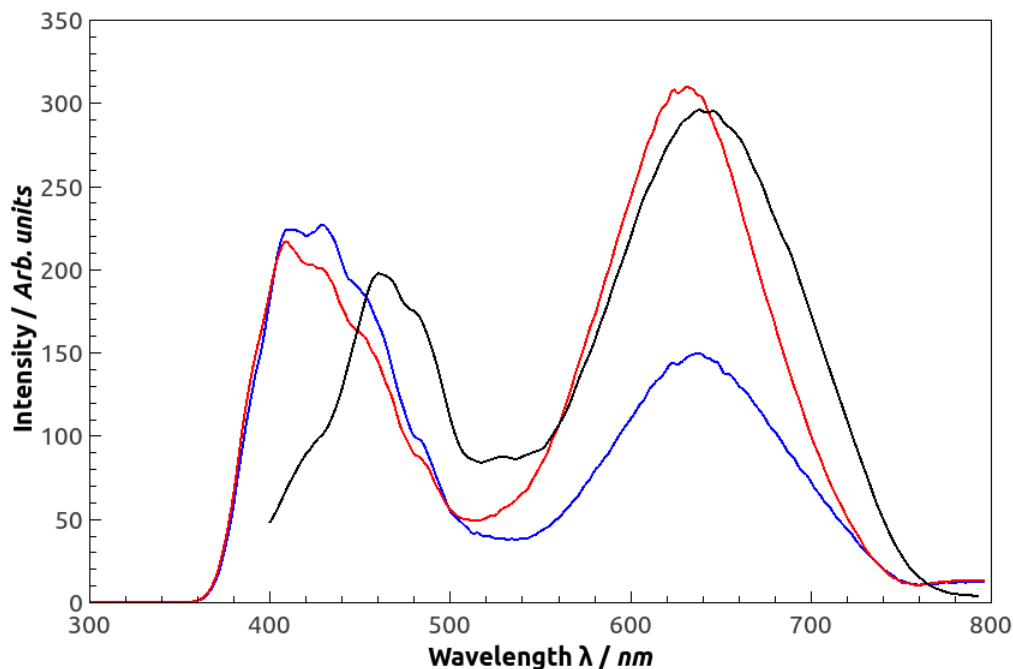


(b) PL spectra for samples of HSiNPs dispersed in distilled toluene, with added alcohols. Control (black line), methanol (red line), and ethanol (blue line).

Figure 20



(c) PL spectra for samples of HSiNPs dispersed in distilled and degassed toluene, with added alcohols. Control (black line), and ethanol (red line).



(d) PL spectra for samples of HSiNPs dispersed in neat toluene, with added phenols. Control (black line), phenol (red line), and tertbutylphenol (blue line).

Figure 20: Plots of the PL spectra for HSiNPs made by electrochemical etching. The four graphs describe the behaviour of the addition of: alcohols to HSiNPs dispersed in neat toluene (a); phenols to HSiNPs dispersed in neat toluene (b); alcohols to HSiNPs dispersed in distilled toluene (c); and alcohols to HSiNPs in distilled and degassed toluene (d).

## 4.2 Time-dependent photoluminescence of HSiNPs

While there are certain immediate changes to the PL when adding solvents to the SiNPs, it is important to monitor these changes over time to determine the rates at which these reactions occur. An example of the changes occurring over time is shown in figure 21, where the intensities of the fitted peaks for a sample of ethanol in neat toluene is monitored. As can be seen in figure 21, the intensity of the peaks increase slightly with time, with the largest increase happening in the red.

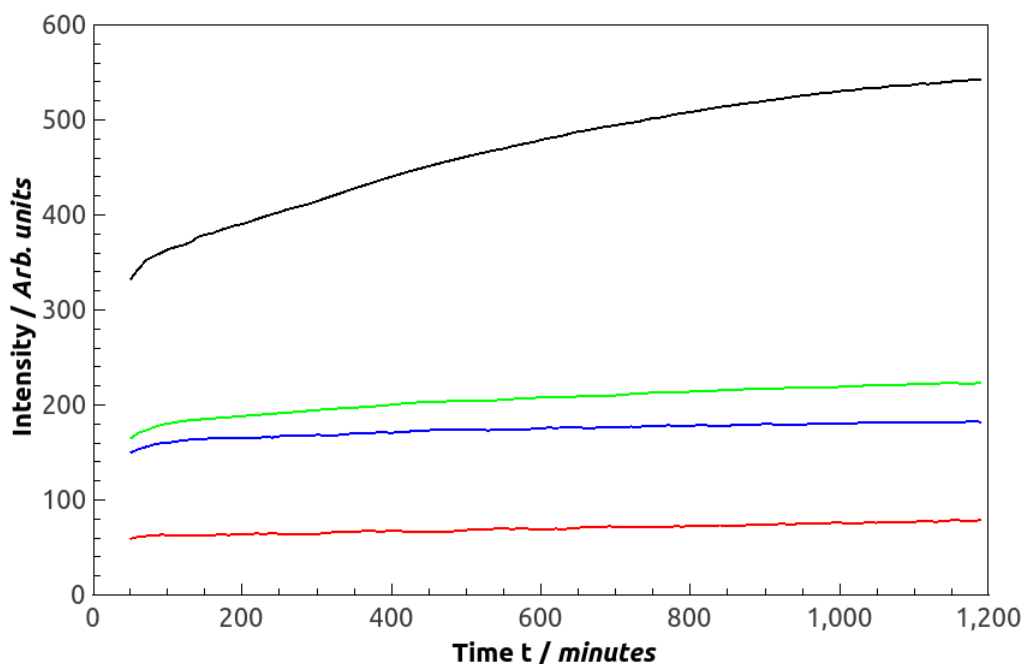


Figure 21: Progression of the intensity of luminescence of peaks  $\alpha$ ,  $\beta$ ,  $\epsilon$ , and  $\zeta$  (red, blue, green, and black lines respectively) with time for a sample of HSiNPs dispersed in neat toluene with added phenol, with a 1-hour moving average.

Time-dependence was performed by measuring the PL spectrum at fixed 10 minute intervals for as long as possible, with measurement times for the experiments varying between 3 and 40 hours depending on availability of the machinery. To account for the noise in the PL a 1-hour moving average was applied to the data. An example of the resulting curves can be seen in figure 21.

By fitting a line through the first hour of data, information about the initial development of the PL can be discovered. Most changes will occur in this period, so analysis will focus on this area. The results are adjusted by dividing by the peak heights (see table 1) in order to remove changes in slope magnitude due to the initial peak height. The results of this analysis can be seen in table 2.

	$\alpha$	$\beta$	$\gamma$	$\delta$	$\epsilon$	$\zeta$
Toluene (neat)		0	0	0	0	0
Toluene (dry)		0.26	2.3	0.11	0.04	0.02
Toluene (dry and degassed)	0.01	0.03			0.03	0
Methanol (neat)		0.49	-0.19	-0.32	2.50	2.11
Methanol (dry)		0.34	-0.28		0.58	0.28
Ethanol (neat)	0.03		0.02	0.02	0.02	0.04
Ethanol (dry)		-0.06	-0.04	0	0.02	0.06
Ethanol (dry and degassed)	0.01	0.01		-0.02	0	0.05
Isopropanol (neat)	0.02		0	-0.04	0.05	0.08
Phenol (neat)	0.20	0.24			0.23	0.25
Tertbutylphenol (neat)	0.19	0.23			0.32	0.12

Table 2: Slope of the intensity change over the first hour of data, in units of intensity per minute (*arb. units / min*).

As can be seen from Table 2, the Toluene-only samples are not changing significantly with time, with the exception of a rapid rise in  $\gamma$  in the case of dry toluene. This is most likely due to oxygen dissolving into the toluene when transferring the sample into the cuvette for analysis. All the samples show no significant change in intensity, with any changes that do occur being due to changes in turbidity. The exception to this is the case of neat toluene, which shows an increase in both  $\epsilon$  and  $\zeta$ .

### 4.3 Discussion

Figure 18a shows a comparison between the three cases where HSiNPs are in the presence of both H<sub>2</sub>O and O<sub>2</sub>; only O<sub>2</sub>; and neither H<sub>2</sub>O nor O<sub>2</sub>. The decrease in red luminescence as H<sub>2</sub>O is removed implies that water is necessary for luminescence in that region. Meanwhile, the increase in blue luminescence under the same conditions, which then decreases once O<sub>2</sub> is also removed implies that O<sub>2</sub> is responsible for the blue luminescence. This is further supported by the fact that the blue luminescence in the control (containing both H<sub>2</sub>O and O<sub>2</sub>) is low, as the reactivity of hydroxide ions formed from water would react more readily with Si than molecular oxygen.

From this it can be hypothesised that the blue luminescence is due to an interaction in the Si-O=O functional group (via adsorption), or its derivatives (such as the Si-O-O-Si peroxide);

### 4.3 Discussion

and the Si-OH functional group causes the red luminescence.

Comparing this result with table 1 it can be seen that the main affected peak is peak  $\beta$ .  $\alpha$  is only present in samples that are dry and degassed, or with molecules larger than methanol present. This suggests that the larger molecules will displace  $O_2$ , therefore allowing the fluorescent decay to occur. It may be that  $\alpha$  and  $\beta$  occur on the same sites, but the  $O_2$  decreases the band gap.

This results refines the result obtained by Dasog *et al*, who claim that oxygen (as well as nitrogen) is the cause of both the reduction in red and the appearance of blue, by showing that while *molecular* oxygen is the cause of blue luminescence, *water* is the cause of the red, and can suppress the blue if present. This is also in accordance with the results obtained in the  $CuCl_2$ -quenched SiNP experiments, which have very low hydroxide levels (see figures 7 on page 17, and 11 on page 20), and very little red luminescence.

Comparing the intensities displayed in figure 20 and table 1, it can be seen that the picture is more complicated than is displayed above, and even within the blue luminescence both water and oxygen play a role. For example,  $\gamma$  - in the 450-470 nm region - decreases on removal of water, but then decreases further once oxygen is removed. The luminescence of this peak is increased on addition of alcohols, which implies that an Si-O-R is providing a pathway for a process that cannot exist if the site is occupied by molecular oxygen or other, electron-withdrawing oxygen-containing compounds.

Similarly to the  $\gamma$ , the small  $\alpha$  is not due to molecular oxygen: it only appears once molecular oxygen has been removed. Indeed, it only exists in samples where either water is present or oxygen is absent, with the exception of the neat toluene and the neat methanol samples, where the peak is not discernable. This could imply that the smaller molecules such as oxygen, water and methanol suppress this peak, but larger molecules on the same site do not interfere with the electronic transitions. It could even be that the larger, more electron-donating molecules aid the decay process on the silicon without directly involving their own energy levels.

The final peak,  $\zeta$ , is perhaps the most important. As mentioned, it arises as a result of the attachment of  $H_2O$  to the SiNP, but addition of other molecules will also change its position and intensity. The increase in intensity when larger alcohols are present suggests that the electron-donating effect is important to the intensity of luminescence. This is especially evident in the case of isopropanol, which contains a large amount of electron-donating 2-propanol.

The most important result of this experiment is that the peaks  $\alpha$ ,  $\beta$ ,  $\gamma$ , and  $\zeta$  are all affected simultaneously. This suggests that they are all due to the same site on the SiNP.

## 5 Conclusions and further work

Alkyl-passivated SiNPs were produced via a cheap, fast, safe and high-yielding one pot, inverse micelle-based method that is easily scalable. This method is an optimisation of previous work which finds additional novelty by virtue of the use of anhydrous copper (II) chloride to quench excess reducing agent present in the system. This addresses the primary flaw previously identified in the method, whereby undesirable alkoxy functionality was observed due to the use of alcohols to quench the excess reducing agent. The resultant particles are in low oxide, highly functionalised and stably passivated, with a strong blue PL. The copper (II) chloride-quenched particles demonstrate a lack of Si–O–C surface functionality as expected. These features are clearly demonstrated via a number of structural, elemental and luminescence spectroscopic techniques. This lack of oxide on the surface makes further chemistry easier to perform, as the number of labile hydride sites is increased.

Further work in this area would focus on exploring other surfactants and continuous phases to produce a portfolio of substances to control size and surface chemistry, as well as work on the stability of these SiNPs in various media. This second piece of work is especially important for applications of SiNPs in harsh environments such as stomach acids and other bodily fluids.

By adding oxygen-containing compounds to dispersions of SiNPs it has been shown that the luminescence of the SiNPs can be controlled. It has also been shown that the intensity of blue luminescence is dependent on the dissolved oxygen in solution and the red luminescence is due to water in solution. Evidence has also been presented to suggest that the red and blue luminescence arises from the same site on the surface of the SiNP. This means that the blue and red luminescence of the nanoparticles can be controlled merely by controlling the ratio of molecular oxygen to water. These colours can also be controlled through the use of oxygen-containing compounds, wherein luminescence can be controlled by careful selection of molecules of certain polarities and sizes. These discoveries make SiNPs more viable as a tool for biomedical imaging.

The work presented here lays the foundation for a number of further areas of research. More experiments need to be performed into the precise relationship between SiNPs and polarity of surface ligands. To begin with, a repeat of these experiments using amides and sulfides may well show that the luminescence can be controlled without the need to rely solely on oxygen-containing compounds. Secondly, more stable ligands must be found that still control the luminescence. This is necessary to prepare SiNPs for use in biological systems, where stability of the nanoparticles is very important. A passivated but still luminescent SiNP can then also be used for more research into the nature of the surface, by looking at suppressing or enhancing the remaining peaks without altering the blue  $\beta$  or red  $\zeta$  peaks.

Indeed, this experiment would be necessary to determine if these two peaks are indeed due to the same site.

## References

- [1] National Nanotechnology Initiative. URL [nano.gov/nanotech-101/what/definition](http://nano.gov/nanotech-101/what/definition).
- [2] P. Walter, E. Welcomme, P. Hallégot, N. J. Zaluzec, C. Deeb, J. Castaing, P. Veysseyre, R. Bréniaux, J. Lévêque, and G. Tsoucaris. Early use of PbS nanotechnology for an ancient hair dyeing formula. *Nano Letters*, 6(10):2215–2219, 2006. ISSN 15306984. doi: 10.1021/nl061493u.
- [3] M. Faraday. The Bakerian Lecture: Experimental Relations of Gold (and Other Metals) to Light, 1857. ISSN 0261-0523.
- [4] DuPont Ti-Pure. Polymers, Light and the Science of TiO<sub>2</sub>.
- [5] K. E. Drexler. The Engines of Creation. *Anchor Books*, 1986. doi: EB I DREX.
- [6] D. M. Eigler and E. K. Schweizer. Positioning single atoms with a scanning tunnelling microscope, 1990. ISSN 0028-0836.
- [7] C. Toumey. Reading Feynman Into Nanotechnology : A Text for a New Science. *Techné*, 12(3):133–168, 2008. ISSN 01617249.
- [8] R. T. Bate. Nanoelectronics. *Nanotechnology*, 1(1):1, 1990. ISSN 0957-4484. doi: 10.1088/0957-4484/1/1/001.
- [9] N. O’Farrell, A. Houlton, and B. R. Horrocks. Silicon nanoparticles: Applications in cell biology and medicine, 2006. ISSN 11769114.
- [10] G. Oberdörster, E. Oberdörster, and J. Oberdörster. Nanotoxicology: An emerging discipline evolving from studies of ultrafine particles, 2005. ISSN 00916765.
- [11] E. Hood. Nanotechnology: Looking as we leap, 2004. ISSN 00916765.
- [12] J. H. Ahire, I. Chambrier, A. Mueller, Y. Bao, and Y. Chao. Synthesis of d-mannose capped silicon nanoparticles and their interactions with MCF-7 human breast cancerous cells. *ACS Applied Materials and Interfaces*, 5(15):7384–7391, 2013. ISSN 19448244. doi: 10.1021/am4017126.
- [13] J. H. Ahire, Q. Wang, P. R. Coxon, G. Malhotra, R. Brydson, R. Chen, and Y. Chao. Highly luminescent and nontoxic amine-capped nanoparticles from porous silicon: Synthesis and their use in biomedical imaging. *ACS Applied Materials and Interfaces*, 4(6): 3285–3292, 2012. ISSN 19448244. doi: 10.1021/am300642m.

## REFERENCES

- [14] Q. Wang, Y. Bao, J. Ahire, and Y. Chao. Co-encapsulation of Biodegradable Nanoparticles with Silicon Quantum Dots and Quercetin for Monitored Delivery. *Advanced Healthcare Materials*, 2(3):459–466, 2013. ISSN 21922640. doi: 10.1002/adhm.201200178.
- [15] S. P. Ashby, J. A. Thomas, P. R. Coxon, M. Bilton, R. Brydson, T. J. Pennycook, and Y. Chao. The effect of alkyl chain length on the level of capping of silicon nanoparticles produced by a one-pot synthesis route based on the chemical reduction of micelle. *Journal of Nanoparticle Research*, 15(2), 2013. ISSN 13880764. doi: 10.1007/s11051-013-1425-8.
- [16] S. P. Ashby, J. García-Cañadas, G. Min, and Y. Chao. Measurement of thermoelectric properties of phenylacetylene-capped silicon nanoparticles and their potential in fabrication of thermoelectric materials. *Journal of Electronic Materials*, 42(7):1495–1498, 2013. ISSN 03615235. doi: 10.1007/s11664-012-2297-x.
- [17] Y. Wang, J. Liu, J. Zhou, and R. Yang. Thermoelectric Transport Across Nanoscale Polymer - Semiconductor - Polymer Junctions. *The Journal of Physical Chemistry C*, 2013.
- [18] F. Lakadamyali and E.n Reisner. Photocatalytic H<sub>2</sub> evolution from neutral water with a molecular cobalt catalyst on a dye-sensitised TiO<sub>2</sub> nanoparticle. *Chemical communications (Cambridge, England)*, 47(6):1695–1697, 2011. ISSN 1359-7345. doi: 10.1039/c0cc04658b.
- [19] F. De Angelis, S. Fantacci, and A. Selloni. Alignment of the dye’s molecular levels with the TiO(2) band edges in dye-sensitized solar cells: a DFT-TDDFT study. *Nanotechnology*, 19(42):424002, 2008. ISSN 0957-4484. doi: 10.1088/0957-4484/19/42/424002.
- [20] Consumer Products Inventory. URL [nanotechproject.org/cpi](http://nanotechproject.org/cpi).
- [21] A. M. Smith and S. Nie. Semiconductor nanocrystals: Structure, properties, and band gap engineering. *Accounts of Chemical Research*, 43(2):190–200, 2010. ISSN 00014842. doi: 10.1021/ar9001069.
- [22] J. Zheng, C. Zhang, and R. M. Dickson. Highly fluorescent, water-soluble, size-tunable gold quantum dots. *Physical Review Letters*, 93(7), 2004. ISSN 00319007. doi: 10.1103/PhysRevLett.93.077402.
- [23] O. Kulakovich, N. Strekal, A. Yaroshevich, S. Maskevich, S. Gaponenko, I. Nabiev, U. Woggon, and M. Artemyev. Enhanced Luminescence of CdSe Quantum Dots

- on Gold Colloids. *Nano Letters*, 2(12):1449–1452, 2002. ISSN 15306984. doi: 10.1021/nl025819k.
- [24] P. R. Coxon, Q. Wang, and Y. Chao. An abrupt switch between the two photoluminescence bands within alkylated silicon nanocrystals. *Journal of Physics D: Applied Physics*, 44(49):495301, 2011. ISSN 0022-3727. doi: 10.1088/0022-3727/44/49/495301.
- [25] Y. Chao, L. Siller, S. Krishnamurthy, P. R. Coxon, U. Bangert, M. Gass, L. Kjeldgaard, S. N. Patole, L. H. Lie, N. O’Farrell, T. A. Alsop, A. Houlton, and B. R. Horrocks. Evaporation and deposition of alkyl-capped silicon nanocrystals in ultrahigh vacuum. *Nature nanotechnology*, 2(8):486–489, 2007. ISSN 1748-3387. doi: 10.1038/nnano.2007.224.
- [26] M. S. Hsieh, N. H. Shiao, and W. H. Chan. Cytotoxic effects of cdse quantum dots on maturation of mouse oocytes, fertilization, and fetal development. *International Journal of Molecular Sciences*, 10(5):2122–2135, 2009. ISSN 14220067. doi: 10.3390/ijms10052122.
- [27] Z. Kang, Y. Liu, C. Tsang, D. Ma, X. Fan, N. Wong, and S. Lee. Water-soluble silicon quantum dots with wavelength-tunable photoluminescence. *Advanced Materials*, 21(6): 661–664, 2009. ISSN 09359648. doi: 10.1002/adma.200801642.
- [28] D. Kovalev, H. Heckler, G. Polisski, J. Diener, and F. Koch. Optical properties of silicon nanocrystals. *Physica Status Solidi B*, 215(2):871–932, 2010. ISSN 09253467. doi: 10.1016/S0925-3467(01)00017-9.
- [29] M. J. Llansola Portolés, P. M. David Gara, M. L. Kotler, S. Bertolotti, E. San Román, H. B. Rodríguez, and M. C. Gonzalez. Silicon nanoparticle photophysics and singlet oxygen generation. *Langmuir*, 26(13):10953–10960, 2010. ISSN 07437463. doi: 10.1021/la100980x.
- [30] M. Dasog, Z. Yang, S. Regli, T. M. Atkins, A. Faramus, M. P. Singh, E. Muthuswamy, S. M. Kauzlarich, R. D. Tilley, and J. G. C. Veinot. Chemical insight into the origin of red and blue photoluminescence arising from freestanding silicon nanocrystals. *ACS Nano*, 7(3):2676–2685, 2013. ISSN 19360851. doi: 10.1021/nn4000644.
- [31] J. Fuzell, A. Thibert, T. M. Atkins, M. Dasog, E. Busby, J. G. C. Veinot, S. M. Kauzlarich, and D. S. Larsen. Red states versus blue states in colloidal silicon nanocrystals: Exciton sequestration into low-density traps. *Journal of Physical Chemistry Letters*, 4(21):3806–3812, 2013. ISSN 19487185. doi: 10.1021/jz401896k.

## REFERENCES

- [32] A. S. Barnard. Modelling of nanoparticles: approaches to morphology and evolution. *Reports on Progress in Physics*, 73(8):086502, 2010. ISSN 0034-4885. doi: 10.1088/0034-4885/73/8/086502.
- [33] J. G. C. Veinot. Synthesis, surface functionalization, and properties of freestanding silicon nanocrystals. *Chemical communications (Cambridge, England)*, (40):4160–4168, 2006. ISSN 1359-7345. doi: 10.1039/b607476f.
- [34] Z. Kang, Y. Liu, and S. Lee. Small-sized silicon nanoparticles: new nanolights and nanocatalysts. *Nanoscale*, 3(3):777–791, 2011. ISSN 2040-3364. doi: 10.1039/c0nr00559b.
- [35] K. A. Littau and P. J. Szajowski. A luminescent silicon nanocrystal colloid via a high-temperature aerosol reaction. *The Journal of Physical Chemistry*, 97:1224–1230, 1993. ISSN 0022-3654. doi: 10.1021/j100108a019.
- [36] U. Woggon, S. Gaponenko, W. Langbein, A. Uhrig, and C. Klingshirn. Homogeneous linewidth of confined electron-hole-pair states in II-VI quantum dots. *Physical Review B*, 47(7):3684–3689, 1993. ISSN 01631829. doi: 10.1103/PhysRevB.47.3684.
- [37] L. T. Canham. Silicon quantum wire array fabrication by electrochemical and chemical dissolution of wafers. *Applied Physics Letters*, 57(10):1046–1048, 1990. ISSN 00036951. doi: 10.1063/1.103561.
- [38] A. H. Mayne, S. C. Bayliss, P. Barr, M. Tobin, and L. D. Buckberry. Biologically interfaced porous silicon devices. *Physica Status Solidi (A) Applied Research*, 182(1): 505–513, 2000. ISSN 00318965. doi: 10.1002/1521-396X(200011)182:1<505::AID-PSSA505>3.0.CO;2-#.
- [39] D. Kovalev, J. Diener, H. Heckler, G. Polisski, N. Künzner, and F. Koch. Optical absorption cross sections of Si nanocrystals, 2000. ISSN 0163-1829.
- [40] F. Priolo, T. Gregorkiewicz, M. Galli, and T. F. Krauss. Silicon nanostructures for photonics and photovoltaics. *Nature nanotechnology*, 9(1):19–32, 2014. ISSN 1748-3395. doi: 10.1038/nnano.2013.271.
- [41] A. P. Alivisatos. Perspectives on the Physical Chemistry of Semiconductor Nanocrystals. *J. Phys. Chem.*, 100(95):13226–13239, 1996. ISSN 0022-3654. doi: 10.1021/jp9535506.

- [42] J. H. Fendler and F. C. Meldrum. The Colloid Chemical Approach to Nanostructured Materials. *Advanced Materials*, 7(7):607–632, 1995. ISSN 0935-9648. doi: 10.1002/adma.19950070703. URL <http://doi.wiley.com/10.1002/adma.19950070703>.
- [43] A. Hagfeldt and M. Graetzel. Light-Induced Redox Reactions in Nanocrystalline Systems. *Chemical Reviews*, 95(1):49–68, 1995. ISSN 0009-2665. doi: 10.1021/cr00033a003.
- [44] W. L. Wilson, P. F. Szajowski, and L. E. Brus. Quantum confinement in size-selected, surface-oxidized silicon nanocrystals. *Science (New York, N.Y.)*, 262(5137):1242–1244, 1993. ISSN 0036-8075. doi: 10.1126/science.262.5137.1242.
- [45] N. Uchida, T. Tada, Y. Ohishi, Y. Miyazaki, K. Kurosaki, and S. Yamanaka. Heavily doped silicon and nickel silicide nanocrystal composite films with enhanced thermoelectric efficiency. *Journal of Applied Physics*, 114(13), 2013. ISSN 00218979. doi: 10.1063/1.4823814.
- [46] J. Wilcoxon, G. Samara, and P. Provencio. Optical and electronic properties of Si nanoclusters synthesized in inverse micelles, 1999. ISSN 0163-1829.
- [47] J. Wang, S. Sun, F. Peng, L. Cao, and L. Sun. Efficient one-pot synthesis of highly photoluminescent alkyl-functionalised silicon nanocrystals. *Chemical communications (Cambridge, England)*, 47(17):4941–4943, 2011. ISSN 1364-548X. doi: 10.1039/c1cc10573f.
- [48] Mai Xuan Dung and Hyun-Dam Jeong. Synthesis of Styryl-Terminated Silicon Quantum Dots: Reconsidering the Use of Methanol. *Bulletin of the Korean Chemical Society*, 33(12):4185–4187, 2012. ISSN 0253-2964. doi: 10.5012/bkcs.2012.33.12.4185. URL <http://koreascience.or.kr/journal/view.jsp?kj=JCGMCS&py=2012&vnc=v33n12&sp=41>
- [49] T. Takagahara. Electron-phonon interactions in semiconductor nanocrystals. *Journal of Luminescence*, 70(1-6):129–143, 1996. ISSN 00222313. doi: 10.1016/0022-2313(96)00050-6.
- [50] L. Mangolini, E. Thimsen, and U. Kortshagen. High-yield plasma synthesis of luminescent silicon nanocrystals. *Nano Letters*, 5(4):655–659, 2005. ISSN 15306984. doi: 10.1021/nl050066y.
- [51] J. C. Vial, A. Bsiesy, F. Gaspard, R. Hérino, M. Ligeon, F. Muller, R. Romestain, and R. M. Macfarlane. Mechanisms of visible-light emission from electro-oxidized

## REFERENCES

- porous silicon. *Physical Review B*, 45(24):14171–14176, 1992. ISSN 01631829. doi: 10.1103/PhysRevB.45.14171.
- [52] T. van Buuren, L. Dinh, L. Chase, W. Siekhaus, and L. Terminello. Changes in the Electronic Properties of Si Nanocrystals as a Function of Particle Size. *Physical Review Letters*, 80(17):3803–3806, 1998. ISSN 0031-9007. doi: 10.1103/PhysRevLett.80.3803.
- [53] T. Kobayashi, T. Endoh, H. Fukuda, S. Nomura, A. Sakai, and Y. Ueda. Ge nanocrystals in SiO<sub>2</sub> films. *Applied Physics Letters*, 71(9):1195, 1997. ISSN 00036951. doi: 10.1063/1.119623.
- [54] G. Belomoin, J. Therrien, and M. Nayfeh. Oxide and hydrogen capped ultrasmall blue luminescent Si nanoparticles. *Applied Physics Letters*, 77(6):779–781, 2000. ISSN 00036951. doi: 10.1063/1.1306659.
- [55] Y. Chao, Q. Wang, A. Pietzsch, F. Hennies, and H. Ni. Soft X-ray induced oxidation on acrylic acid grafted luminescent silicon quantum dots in ultrahigh vacuum. *Physica Status Solidi (A) Applications and Materials Science*, 208(10):2424–2429, 2011. ISSN 18626300. doi: 10.1002/pssa.201127212.
- [56] F. Erogbogbo, K. Yong, I. Roy, G. Xu, P. N. Prasad, and M. T. Swihart. Biocompatible luminescent silicon quantum dots for imaging of cancer cells. *ACS nano*, 2(5):873–878, 2008. ISSN 1936-086X. doi: 10.1021/nn700319z.
- [57] J. H. Warner, A. Hoshino, K. Yamamoto, and R. D. Tilley. Water-soluble photoluminescent silicon quantum dots. *Angewandte Chemie - International Edition*, 44(29):4550–4554, 2005. ISSN 14337851. doi: 10.1002/anie.200501256.
- [58] R. M’Ghaïeth, H. Maâref, I. Mihalcescu, and J. C. Vial. Porous silicon: photoluminescence decay in the nanosecond range. *Microelectronics Journal*, 30(7):695–698, 1999. ISSN 00262692. doi: 10.1016/S0026-2692(99)00013-0.
- [59] M. Wolkin, J. Jorne, P. Fauchet, G. Allan, and C. Delerue. Electronic States and Luminescence in Porous Silicon Quantum Dots: The Role of Oxygen, 1999. ISSN 0031-9007.